Variable-Rate, Variable-Power Network-Coded-QAM/PSK for Bi-Directional Relaying Over Fading Channels

Yanping Yang, *Student Member, IEEE*, Wei Chen, *Senior Member, IEEE*, Ou Li, and Lajos Hanzo, *Fellow, IEEE*

***Abstract*—Network coded modulation (NCM) holds the promise of significantly improving the efficiency of two-way wireless relaying. In this contribution, we propose near instantaneously adaptive variable-rate, variable-power QAM/PSK for NC-aided decode-and-forward two-way relaying (DF-TWR) to maximize the average throughput. The proposed scheme is optimized subject to both average-power and bit-error-ratio (BER) constraints. Based on the BER bounds, we investigate a discrete-rate adaptation scheme, relying on a pair of solutions proposed for maximizing the spectral efficiency of the network. We then derive a closed-form solution based power adaptation policy for a continuous-rate scheme and quantify the signal-to-noise ratio (SNR) loss imposed by NC-QAM. Our simulation results demonstrate that the proposed discrete adaptive NC-QAM/PSK schemes are capable of attaining a higher spectral efficiency than their fixed-power counterparts.**

***Index Terms*—Network coded modulation, adaptive modulation, two-way relaying, fading channels, spectral efficiency.**

I. Introduction

TWO-WAY relaying (TWR), also known as bi-directional relaying, constitutes an appealing technique of improving the throughput of the existing wireless network. The landmark contribution of Li, Yeung and Cai [1] put forward the linear Network Coding (NC) concept for single-source multicast networks for the sake of approaching the max-flow bound of the information transmission rate. Inspired by this work, a variety of NC methods have been proposed [2]–[9]. To the best of our knowledge, [2] was the first contribution that combined NC with the physical layer broadcast capability of the wireless medium, which is capable of improving the achievable throughput with the aid of the modulo-two based superposition of sequences. From an information theoretic view, Wu [3] and Xie [4] investigated the downlink (DL) capacity of asymmetric Decoded-and-Forward Two-Way Relaying (DF-TWR). More practically, NC was jointly designed with superposition coding in [5], where the authors proposed a cross-layer method for joint interference cancellation and network coding in multihop wireless networks, which may substantially improve the capacity regions, whilst reducing the power dissipated at the relay node. Symbol level NC was investigated in [6], which is capable of improving the asymmetric[1] relay throughput using hierarchical modulation. The joint design of NC and modulation was investigated in [7], which alleviated the asymmetric relaying-induced problems in TWR networks. Based on a set-partitioning algorithm, both NC-QAM/PSK and a NC oriented maximum ratio combining (MRC) technique was conceived for improving both the throughput as well as the achievable spatial diversity gain at a low complexity [8], [9], which circumvented the asymmetric transmission problems of DF-TWR. For the sake of maximizing the data rates of two-way links under certain BER constraints, constant-power, variable-rate adaptive Network-Coded Modulation (NCM) was proposed in [8]. This motivates our research on how to design variable-power, variable-rate adaptive NCM for TWR, because it is beneficial to consider joint power and rate allocation schemes for time-varying fading channels.

Inspired by the above-mentioned solutions, improving the spectral efficiency for transmission over fading channels has gradually become the focus of the related research [10]–[17]. As one of the key techniques that has found its way into both current and future wireless systems, adaptive modulation has received extensive attentions. Hanzo *et al.* designed diverse near-instantaneously adaptive modulation techniques in [10]–[12]. Based on Shannon capacity and BER bounds, Goldsmith *et al.* [13]–[15] investigated point-to-point adaptive modulation schemes for flat-fading channels, where both the data rate and the transmit power were near-instantaneously adapted for the sake of maximizing the spectral efficiency, whilst maintaining a constant BER. In [16], constant-power single- and multicarrier adaptive quadrature amplitude modulation (AQAM) was

Manuscript received March 28, 2014; revised July 22, 2014; accepted August 26, 2014. This paper was supported in part by the National Basic Research Program of China (973 Program) under Grant 2013CB336600, by NSFC Excellent Young Investigator Award 61322111, by NSFC Project 61201380, by the National High Technology Research and Development Program of China (863 Program) under Grant 2012AA121606, by the National Innovative Talents Promotion Program 2013RA2151, by the MoE New Century Talent Program NCET-12-0302, by Beijing Nova Program Z121101002512051, and by the National Science and Technology Key Project 2013ZX03003006-005. The associate editor coordinating the review of this paper and approving it for publication was J. Yuan.

Y. Yang is with the National Digital Switching System Engineering and Technological R&D Center, Zhengzhou 450002, China. He is also with the Department of Electronic Engineering, Tsinghua University, Beijing 100084, China (e-mail: y.p.yang1986@gmail.com).

W. Chen is with the Department of Electronic Engineering, Tsinghua University, Beijing 100084, China (e-mail: wchen@tsinghua.edu.cn).

O. Li is with the National Digital Switching System Engineering & Technological R&D Center, Zhengzhou 450002, China (e-mail: zzliou@126.com).

L. Hanzo is with the School of Electronics and Computer Science, University of Southampton, Southampton SO17 1BJ, U.K. (e-mail: lh@ecs.soton.ac.uk).

Digital Object Identifier 10.1109/TCOMM.2014.2354353

[1]The asymmetry here implies that the two-way traffic flows may have different symbol rates.

investigated compared to variable-power variable-rate M-ary QAM (MQAM) proposed in [15]. Following the similar approach of [15], Liu *et al.* developed a cross-layer design in [17], which combines adaptive modulation and coding at the physical layer combined with a truncated Automatic Repeat reQuest (ARQ) protocol at the data link layer. These adaptive modulation contributions studied single-user transmission, relying on a single channel's quality. This motivates us to intrinsically amalgamate adaptive modulation with TWR where the downlink streaming from the relay (R) to both destinations (D) has to simultaneously adapt to a pair of channel conditions.

Since the R-D DL of TWR is equivalent to the classic broadcast channel (BC) relying on side information, we consult the relevant literature on adaptive modulation conceived for both broadcast channels and for multicast systems [18]–[22]. Specifically, the authors of [18] investigated both the achievable channel capacity and the power allocation of the downlink of time-varying TWR. The resource allocation of multicast systems was discussed in [19]–[21], while the adaptive modulation aided multiple-input, multiple-output (MIMO) downlink channel was studied in [22]. To the best of our knowledge, there is a paucity of contributions on the joint power and rate allocation of near-instantaneously adaptive NCM schemes designed for broadcast channels or multicast systems. This is because the BC channel has to dispense with power adaptation at the transmitter without the knowledge of the users' channel state information (CSI). However, gleaming perfect CSI for a large user-population is unrealistic in broadcast channels or multicast systems. Therefore, the transmitter usually transmits its messages at a fixed power and using fixed modulation modes, rather than implementing power adaptation. However, in the downlink of TWR, there are only two users. Therefore the two user's accurate CSI can be relatively easily obtained at the relay node. Hence we embark on investigating the two users' joint power and rate allocation problem in the context of TWR by relying on perfect CSI.

Therefore we take the challenge of designing joint power and rate adaptation aided NCM for the DF-TWR DL relying on side information. Compared to the conventional single-user adaptive modulation scheme of [15], the main differences can be summarized as follows:

i) Instead of a single channel, the power allocation strategy of our proposed scheme has to simultaneously adapt to a pair of channel conditions;
ii) The pair of R-D links are coupled due to the SNR loss imposed by NC-QAM, which implies that the user who has a lower transmit rate will suffer from an SNR loss [8];
iii) When we investigate a discrete-rate adaptive scheme, a specific transmit power results in two different transmit rates, depending on the two links' CSI. However, the power and the two rates cannot be optimally matched. Explicitly, when one user achieves its optimal power and rate match, it is highly likely that for the other user, the power will be higher than the user's modulation mode actually needs at this moment, which implies that there is a power-loss. Alternatively at a given power this may be viewed as a rate-loss. By contrast, in [15], the power and rate allocation is always optimal. In conclusion, the combination of joint power and rate adaptive modulation aided NCM requires more sophisticated design than that of conventional single-user adaptive modulation.

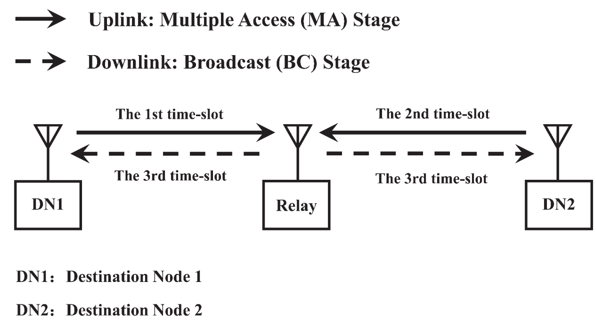

Fig. 1. System model of DF-TWR (Three-timeslot TWR).

Based on the idea of intrinsically amalgamating NCM and adaptive modulation, we propose near-instantaneously adaptive NC-QAM/PSK for the downlink of DF-TWR, which can be regarded as a joint optimization with the objective of maximizing the capacity of networks. As the RN simultaneously broadcasts its signals to two receiver nodes, the same transmit power has to adapt to both fading channel conditions. Therefore the key challenge for the scheme is to optimize both the transmit power and the transmit rates for the sake of maximizing the achievable spectral efficiency, while satisfying the average power and BER constraints. To solve this optimization problem, firstly, we proposed a solution for a discrete-rate scheme based on the so-called fading region partitioning method. Secondly, a closed-form solution is derived for the power adaptation policy of a continuous-rate adaptive scheme. Finally, on the basis of this continuous-rate solution, we conceive another discrete-rate scheme by invoking a continuous-rate discretization method. Based on the above arguments it may be concluded that the most significant contribution of this paper is the joint adaptive allocation of power and rate for NCM. The proposed adaptive NC-QAM/PSK scheme conceived for DF-TWR is capable of beneficially improving the achievable spectral efficiency, therefore holds the promise of rich near-future applications.

The rest of this paper is organised as follows. Section II presents our system model, while Section III describes our unified adaptive NCM optimization problem, followed by a pair of discrete-rate solutions proposed for practical scenarios which are applicable to arbitrary constellations. Section IV presents our simulation results for characterizing our adaptive NC-QAM/PSK, while our concluding remarks are provided in Section V.

II. System Model

Consider the DF-TWR network associated with a multicarrier system, which employs time division duplexing. Fig. 1 shows an abridged general view of a three-timeslot bidirectional transmission system, which includes two destination nodes and a relay node. Destination node 1 (DN1) and DN2 in the DL also act as source nodes (SN) during the uplink transmission stage. The information exchange between the two DNs can be divided into two distinct stages: the multiple access (MA) stage when the two nodes separately send their data to the

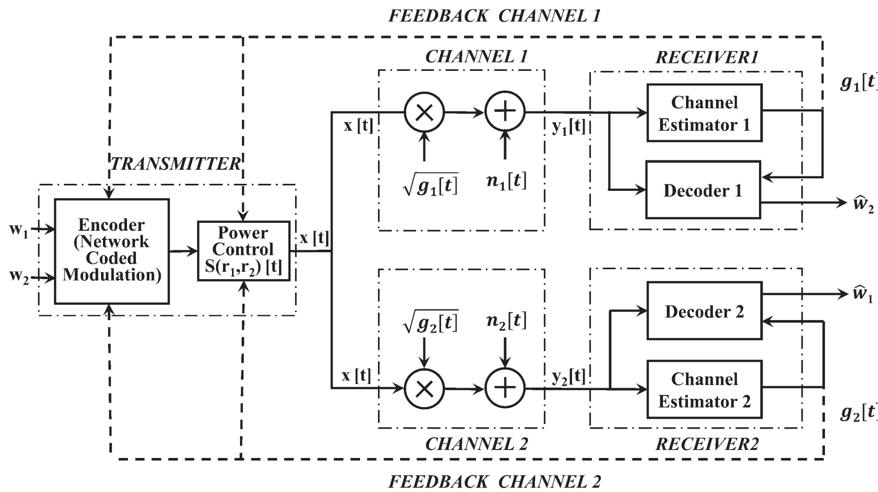

Fig. 2. System model of adaptive NC-QAM/PSK for DF-TWR.

relay, and the broadcast (BC) stage, when the relay broadcasts the combined signal to both DN1 and DN2. Each DN has *a priori* knowledge of its own message intended for the other.

Based on the above-mentioned TWR model, we then construct the adaptive NC-QAM/PSK system model of Fig. 2, where the key part of the scheme is the transmitter design, constituted by the NCM design and the adaptive modulation design. Since the fixed-mode NCM has already been richly studied in [8], we focus our attention on adaptive NCM conceived for near-instantaneously time-varying fading channels. Accordingly, we describe the system model of adaptive NC-QAM/PSK.

Before introducing the system's structure, we first list the assumptions adopted in this paper:

A1) The channel is a non-dispersive and slowly-varying Rayleigh fading channel. When the channel is changing faster than it can be estimated and fed back to the transmitter, adaptive techniques will perform poorly.

A2) Perfect channel state information (CSI) is available both at the relay as well as at DN1 and DN2 using training-based channel estimation. The idealized simplifying assumption that the feedback path does not introduce any errors and has no latency may be approximately satisfied by using a low-delay feedback link relying on powerful error control. The practical system design relying on delayed or noisy CSI [15] is left for our future investigations.

A3) Linear modulation is used, where the adaptation takes place at integer multiples of the symbol rate of $R_s = 1/T_s$, where T_s denotes the symbol duration. It is also assumed that the system uses ideal Nyquist criterion, having a bandwidth of $B = 1/T_s$. We assume having a non-dispersive discrete-time downlink channel having stationary ergodic time-varying gains of $\sqrt{g_i[t]}, i = 1, 2$ contaminated by the additive white Gaussian noise (AWGN) $n_i[t]$, where t denotes the time instants.

We conceive the NCM design according to [8]. In this paper, we only focus our attention on the DL of DF-TWR, where the messages at the RN are processed and broadcast to DN1 and DN2 using NC-QAM/PSK. In the static asymmetric DF-TWR DL, the equivalent baseband signals received at the coherent receiver of DN1 and DN2 are represented by

$$Y_i = h_i X + Z_i, i = 1, 2, \tag{1}$$

where the channel gains are denoted by $|h_i|^2 = g_i$, with g_i representing the power gains. The transmit symbol at the RN is denoted by X, while Z_i represent the AWGN at DN1 and DN2.

Without loss of generality, we assume that the transmit constellation sizes are denoted by M_1, M_2, let $M_2 \geq M_1$, $M_2/M_1 = \mathbb{N}$. The messages w_1, w_2 to be transmitted from the pair of source nodes will be merged into a single signal (denoted by X) using the modulo-two operation at the relay [8]. For QAM, the messages w_1, w_2 then will be respectively mapped to symbols from the set of M-ary QAM constellation points, which is formulated as

$$\chi_i = \left\{2\sqrt{M_i}\left(a_i^I + j a_i^Q\right) - \left(\sqrt{M_i} - 1\right)(1+j) : a_i^I, a_i^Q \in \mathcal{A}_i\right\}, \tag{2}$$

where

$$\mathcal{A}_i = \begin{cases} \left\{0, \frac{1}{2}\right\}, & \text{if } M_i = 4 \\ \left\{0, \frac{1}{\sqrt{M_i}}, \frac{2}{\sqrt{M_i}}, \ldots, \frac{\sqrt{M_i}-1}{\sqrt{M_i}}\right\}, & \text{if } M_i > 4 \end{cases}, \quad i = 1, 2 \tag{3}$$

where $M_i \in \{4, 16, 64, \ldots\}$ for QAM. Given the normalised amplitudes (a_1^I, a_1^Q) and (a_2^I, a_2^Q), the transmitter will generate the NC-QAM symbol as

$$X = d\left[2\sqrt{M_2}(a^I + j a^Q) - \left(\sqrt{M_2} - 1\right)(1 + j)\right], \tag{4}$$

where we have $d = \sqrt{((3E_s)/2(M_2 - 1) - 1))}$, $M_2 > M_1$, while d denotes half of the symbol-distance in QAM, given an energy of E_s per symbol. The normalised amplitudes are given by

$$\begin{cases} a^I = a_1^I + a_2^I, \bmod 1 \\ a^Q = a_1^Q + a_2^Q, \bmod 1. \end{cases} \tag{5}$$

For NC-PSK, w_1, w_2 will be mapped to the symbols χ_1, χ_2 chosen from a normalised M-ary PSK (MPSK) constellation, as in $\chi_i = \{\cos\theta_i + j\sin\theta_i : \theta_i \in \Theta_i\}$, where we have

$$\Theta_i = \left\{0, \frac{2\pi}{M_i}, \ldots, \frac{2(M_i - 1)\pi}{M_i}\right\}, \quad i = 1, 2, \tag{6}$$

where $M_i \in \{2, 4, 8, 16, \ldots\}$ for PSK. Given the phases θ_1 and θ_2, the transmitter generates an NC-PSK symbol given by

$$X = \sqrt{E_s}\left(\cos\theta + j\sin\theta\right), \tag{7}$$

where E_s denotes the symbol energy, while the symbol's phase θ is given by

$$\theta = \theta_1 + \theta_2 \mod 2\pi. \tag{8}$$

We then conceive near-instantaneously adaptive NCM for time-varying fading channels where the modulated signals will be represented by the signal sequence in the system model of Fig. 2. Therefore the previous symbol X will be represented as $x[t]$, while Y will be represented by $y_i[t], i = 1, 2$.

Let us now describe our adaptive transmission scheme seen in Fig. 2. We consider discrete-time (t denotes discrete time instants) flat fading channels adhering to the assumptions A1)–A3), where the transmitter (relay) dynamically adjust both its transmit power and transmit rates according to the power gains $g_1[t]$ and $g_2[t]$ signalled to it from the two receivers (DN1 and DN2). Let us denote the average transmit power by $\overline{S}$, the noise density of $n_i[t]$ by $(N_0/2)$, the channel gain by $g_i[t]$ and the average channel gain by $\overline{g}$. For a constant transmit power $\overline{S}$, the instantaneous received SNRs are $\gamma_i[t] = \overline{S}g_i[t]/(N_{0_i}B)$. Upon normalization by $\overline{S}$, we can assume that $\overline{g} = 1$. Then the average received SNRs are $\overline{\gamma}_i = \overline{S}/(N_{0_i}B)$. We denote the probability distribution of the received SNR by $p(\gamma_i) = p(\gamma_i[t] = \gamma_i)$. In this paper, the fading distributions $p(\gamma_i)$ are assumed to be either lognormal or exponential (Rayleigh fading). When the context is unambiguous, we will omit the time reference t related to n_i, g_i, γ_i and $\overline{\gamma}_i$.

The above-mentioned two designs constitute the fundamental framework of our adaptive NC-QAM/PSK scheme. Specifically, the assumption of A2) signifies that the feedback channel is error free and has no latency, which could be at least approximately satisfied by using a fast feedback link with powerful error control for feedback information. The feedback path delays are not shown in Fig. 2.

III. Adaptive Network Coded M-ary Modulation

In Section II we discussed the general system model of adaptive NC-QAM/PSK. In this section we will describe the specific form of adaptive NC-QAM/PSK aided DF-TWR, where both the rate and the transmit power of M-ary QAM/PSK are varied near-instantaneously for the sake of maximizing the spectral efficiency, while meeting the BER targets. We study this specific form of adaptive NCM in the context of the downlink of DF-TWR. Therefore, the main emphasis of this paper is on practical adaptive modulation and on its spectral efficiency normalized to the theoretical maximum. The remainder of this section is organized as follows. In Subsection A, we describe the optimization problem of our variable-rate, variable-power NC-QAM/PSK scheme. The spectral efficiency of our discrete-rate, continuous-power scheme is discussed in Subsection B. We then investigate the continuous-rate, continuous-power adaptive scheme in Subsection C. Finally, we propose a continuous-rate discretization method in Subsection D. Before analyzing our adaptive schemes, we would like to first list some of the notations used.

- $M_i(\gamma_i)$: denotes the constellation sizes that are used in the continuous-rate scheme (Section III-C), with their domains being $M_i(\gamma_i) \geq 1$.
- $M_{1,\eta}$, $M_{2,\delta}$: denotes the constellation sizes that are used in discrete-rate schemes (Section III-B and D), which implies that receiver 1 (or 2) adopt the transmission modes η (or δ). Usually their values are discrete and are larger than 2.
- $k(\gamma_i)$: denotes the continuous transmit rates.
- $k_{1,\eta}$, $k_{2,\delta}$: denotes the discrete transmit rates.
- λ_i. denotes the SNR-loss imposed by NC-QAM. We included the derivation of SNR-loss in the Appendix.
- $S(\gamma_1, \gamma_2)$: denotes the continuous instantaneous transmit power, which is related to instantaneous SNR γ_1 and γ_2.
- $S_{\eta\delta}(\gamma_1, \gamma_2)$: denotes the discrete instantaneous transmit power, which corresponds to the transmission modes η and δ.
- ω_i: denotes the weighting coefficients of the relay-DN1 link and relay-DN2 link, respectively.

A. Unified Problem Formulation for Adaptive NC-QAM/PSK

Again, the emphasis of this contribution is on the transmitter design relying on the CSI knowledge, therefore it is necessary to derive the basic formulas required for the transmitter's design. Based on these formulas we unify the basic optimization problem for adaptive NC-QAM/PSK, which will be discussed in Subsections B, C and D.

1) The Achievable Rate for the Downlink of the TWR: According to Section II, when the time reference t can be omitted, without any ambiguity we may rewrite the expression of the corresponding parameters as $\gamma_i, i = 1, 2$, $\overline{\gamma}_i$ and $p(\gamma_i)$, which will be used in deriving the system's capacity. The capacity of fading channels for DF-TWR is limited by both the transmit power and bandwidth available. Let $S(\gamma_1, \gamma_2)$ denote the transmit power relative to the instantaneous SNR γ_1 and γ_2, subject to the average power constraint of

$$\int_0^\infty \int_0^\infty S(\gamma_1, \gamma_2)p(\gamma_1)p(\gamma_2)d\gamma_1 d\gamma_2 = \bar{S}, \tag{9}$$

where $p(\gamma_1)$ is independent of $p(\gamma_2)$. When considering a Rayleigh fading channel for example, we have

$$p(\gamma_i) = \frac{1}{\overline{\gamma_i}} e^{-\gamma_i/\overline{\gamma_i}}, \quad i = 1, 2, \tag{10}$$

where $\overline{\gamma_i} = \overline{S}T_s/N_0 = \overline{E_s}/N_0$ denotes the average SNR per symbol, $T_s = 1/B$.

The BER performance of NC-QAM/PSK matches well with the theoretical BER expressions provided in [8], [23]. However, the theoretical BER expressions contain the Q-function [24], which is hard to invert. In our proposed adaptive NC-QAM/PSK scheme, we use Error Probability Bounds (EPBs) ([23, Chapter 9]) instead of the theoretical BER expressions ([23, Table 6.1]). Particularly, NC-QAM exhibits a modest SNR loss, when the selected constellation sizes of the DN1 and DN2 are different [8]. Therefore the concept of the SNR-loss coefficients λ_1, λ_2 will be introduced into our BER expressions. However, there is no SNR-loss for NC-PSK [8]. To unify these expressions, we introduce the same coefficients, but let $\lambda_1 = \lambda_2 = 1$ for NC-PSK.

The unified approximation BER bound has been provided in [23, Chapter 9.4]. If we consider the above-mentioned SNR-loss and write the BER bound [23] in a pairwise form, then we arrive at:

$$\begin{cases} P_{b_1}(\gamma_1) \le c_1 \exp\left[\frac{-c_2\lambda_1\gamma_1\frac{S(\gamma_1,\gamma_2)}{\bar{S}}}{2^{c_3 k(\gamma_1)}-c_4}\right] \\ P_{b_2}(\gamma_2) \le c_1 \exp\left[\frac{-c_2\lambda_2\gamma_2\frac{S(\gamma_1,\gamma_2)}{\bar{S}}}{2^{c_3 k(\gamma_2)}-c_4}\right], \end{cases} \tag{11}$$

where c_1, c_2 and c_3 are fixed positive constants, while c_4 is a real constant. The received SNRs now become $\gamma_i S(\gamma_1, \gamma_2)/\bar{S}$, $i = 1, 2$. The transmit rates $k(\gamma_1)$, $k(\gamma_2)$ hence become

$$k(\gamma_i) = \frac{\log_2 M_i(\gamma_i)}{c_3}, \quad i = 1, 2, \tag{12}$$

where $M_i(\gamma_i)$ represents the constellation sizes, while the SNR-loss coefficients λ_1 and λ_2 are

$$\lambda_i = \begin{cases} \frac{1-M_i^{-1}(\gamma_i)}{1-M_1^{-1}(\gamma_1)}, \text{if } M_1(\gamma_1) \ge M_2(\gamma_2) \ge 1, i = 1, 2 \\ \frac{1-M_i^{-1}(\gamma_i)}{1-M_2^{-1}(\gamma_2)}, \text{if } M_2(\gamma_2) \ge M_1(\gamma_1) \ge 1, i = 1, 2 \\ 1, \; NC-PSK scheme. \end{cases} \tag{13}$$

The SNR-loss coefficients are obtained according to Paragraph 1, Line 10 of the Appendix, where for the sake of streamlining the related formula, we let $\lambda_1 = \lambda_2 = 1$ for NC-PSK. Of particular note is that in Eq. (13), the values of the constellation sizes $M_1(\gamma_1)$ and $M_2(\gamma_2)$ are continuous, with their domains being $[1, \infty)$.

From Eq. (13) we see that when the MQAM constellation sizes $M_1(\gamma_1)$ and $M_2(\gamma_2)$ are fixed and different, an SNR loss is imposed at the destination node having a lower-order constellation size. Fortunately, the SNR loss decreases upon increasing the receiver-side SNR, which means that higher-order modulations can be used. We will carry out the related analysis according to the different scenarios in the subsequent subsections.

Throughout this paper, the BER bounds of MQAM are given by ([23, Eqs. (9.6) and (9.7)]), where we have $c_1 = 2$ or 0.2, $c_2 = 1.5$, $c_3 = 1$ and $c_4 = 1$. The SNR-loss coefficients $\lambda_i, i = 1, 2$ are given by Eq. (13). By contrast, the BER bound of MPSK is given by ([23, Eq. (9.49)]), with $c_1 = 0.05$, $c_2 = 6$, $c_3 = 1.9$, $c_4 = 1$. Specifically, we have $\lambda_i = 1, i = 1, 2$ for MPSK.

To facilitate our forthcoming discussions and calculations, Eq. (11) may be reformulated as

$$M_i(\gamma_i) \le c_4 + K_i\lambda_i\gamma_i\frac{S(\gamma_1, \gamma_2)}{\bar{S}}, \; i = 1, 2, \tag{14}$$

where

$$K_i = -\frac{c_2}{\ln(P_{b_i}/c_1)}. \tag{15}$$

These BER bounds may be expected to closely approximate the accurate BER expressions and may also be readily inverted. Therefore we can obtain $M_i(\gamma_i)$ or $k(\gamma_i)$ as a function of P_{b_i} and $S(\gamma_1, \gamma_2)$.

2) Variable-Rate, Variable-Power NC-QAM/PSK: Let us now discuss the capacity of variable-rate, variable-power NC-QAM/PSK for the downlink of DF-TWR. As seen in Fig. 2, in a fading channel where the relay broadcasts its signals to both DN1 and DN2, the receiver side SNR γ_1, γ_2 fluctuates as a function of time. We adjust $S(\gamma_1, \gamma_2)$ according to γ_1, γ_2, under the average power constraint of $\bar{S}$.

Our optimization problem is then formulated as that of maximizing the spectral efficiency of adaptive NCM. Let $R[\gamma_1, \gamma_2, S(\gamma_1, \gamma_2)]$ denote the available rate as a function of γ_1, γ_2 and $S(\gamma_1, \gamma_2)$, which is expressed as

$$R\left[\gamma_1, \gamma_2, S(\gamma_1, \gamma_2)\right] = \sum_{i=1}^{2} \frac{\omega_i}{c_3} \log_2 M_i(\gamma_i), \quad i = 1, 2, \tag{16}$$

where $M_i(\gamma_i)$ is given by Eq. (14), ω_1 denotes the significance of the DN1 channel, while that of the DN2 channel is ω_2. Naturally, we have $\omega_1 + \omega_2 = 1$ and $0 \le \omega_i \le 1, i = 1, 2$.

The achievable spectral efficiency is obtained by integrating the rate function over the fading region D. We then unify the optimization problem as follows:

$$\begin{aligned} &\text{maximize } \frac{R}{B} = \iint_D R[\gamma_1, \gamma_2, S(\gamma_1, \gamma_2)]p(\gamma_1)p(\gamma_2)d\gamma_1 d\gamma_2 \\ &\text{subject to } \iint_D S(\gamma_1, \gamma_2)p(\gamma_1)p(\gamma_2)d\gamma_1 d\gamma_2 = \bar{S} \\ &\qquad S(\gamma_1, \gamma_2) \ge 0 \\ &\qquad D = \mathbb{R}^2, \end{aligned} \tag{17}$$

where $\bar{S}$, $S(\gamma_1, \gamma_2)$, γ_i, B, $p(\gamma_i)$ were defined as that of our system model.

Since the logarithmic functions in Eq. (16) are concave and so is their sum, Eq. (17) constitutes a convex optimization problem. We form the Lagrangian by exploiting the Karush–Kuhn–Tucker (KKT) condition similarly to the approach of [18], where υ^* and μ^* are Lagrange multipliers. In particular, for the discrete-rate scheme, the integration area D is divided into sub-areas denoted by $D_{\eta,\delta}$, which are used as our optimization variables.

We are now in the position to conceive two different adaptive schemes, namely a discrete-rate, continuous-power NC-QAM/PSK and a continuous-rate, continuous-power NC-QAM/PSK arrangement. For the former optimization problem, not only the transmit power adaptation policy, but also the fading region division requires further discussions. For the latter scheme, we just have to find the optimal power adaptation policy that maximizes the achievable spectral efficiency, which is formulated as Eq. (18), shown at the bottom of the next page.

Eq. (17) presents a general formulation of the adaptive NC-QAM/PSK optimization problem. In the following subsections, both the discrete-rate, continuous-power and the continuous-rate, continuous-power adaptive schemes will be investigated in detail.

B. Discrete-Rate Adaptive M-ary QAM/PSK

According to the optimization problem formulated in the previous subsection, we conceive a practical solution for adaptive NC-QAM/PSK, which is referred to as our discrete-rate, continuous-power DF-TWR scheme. Explicitly, in the traditional single-user continuous-rate adaptation scheme we have to find the optimal cutoff fade depth parameter υ^*[15], whilst in the proposed discrete-rate schemes, our goal is that of finding the joint optimal power and rate for the pair of independent fading distributions of the relay-DN1 and relay-DN2 links. This issue will be discussed first, followed by a solution for our discrete variable-rate, variable-power NC-QAM/PSK scheme.

Similarly to our previous system model, the BER bounds of Eq. (11) and its rearranged form in Eq. (14) constitute the basis of our discussions. In the joint-optimization scheme destined for the receivers DN1 and DN2, the transmit rates are denoted by $k_{1,\eta}$ and $k_{2,\delta}$, which directly depend on the constellation sizes $M_{1,\eta}$ and $M_{2,\delta}$ as follows:

$$\begin{cases} k_{1,\eta} = \frac{\log_2 M_{1,\eta}}{c_3} \\ k_{2,\delta} = \frac{\log_2 M_{2,\delta}}{c_3}. \end{cases} \tag{19}$$

For each receiver side at DN1 and DN2, we adopt the single-user partitioning method of [15]. Specifically, we consider the discrete sets of MQAM/MPSK transmission modes $\mathcal{M}_1 = \{M_{1,0}, \ldots, M_{1,N_1-1}\}$, $\mathcal{M}_2 = \{M_{2,0}, \ldots, M_{2,N_2-1}\}$, with $M_{1,0} = 0$ and $M_{2,0} = 0$ implying no transmission. The receiver-side SNR distributions are then divided into N_1 and N_2 fading-magnitude regions denoted by $R_{1,n_1} = [\gamma_{1,n_1-1}, \gamma_{1,n_1}), n_1 = 0, \ldots, N_1-1$, $R_{2,n_2} = [\gamma_{2,n_2-1}, \gamma_{2,n_2}), n_2 = 0, \ldots, N_2-1$, where $\gamma_{i,-1} = 0, \gamma_{i,N_i-1} = \infty, i = 1, 2$. We then activate the pair of fixed constellation sizes of M_{1,n_1}, M_{2,n_2}, when the receiver side SNRs obey $\gamma_1 \in R_{1,n_1}$, $\gamma_2 \in R_{2,n_2}$.

According to the above fading-magnitude partitioning method and to the basic optimization problem of Eq. (17), we have now formulated our basic discrete-rate scheme for DF-TWR. The associated power control policy conceived for joint-optimization should now be discussed further. Let $S_{\eta\delta}(\gamma_1, \gamma_2), \eta \in \{0, 1, \ldots, N_1-1\}$, $\delta \in \{0, 1, \ldots, N_2-1\}$ denote the relay's transmit power for $\gamma_1 \in R_{1,n_1}$, $\gamma_2 \in R_{2,n_2}$. From Eq. (14) we arrive at:

$$\begin{cases} \frac{S_{\eta\delta}(\gamma_1,\gamma_2)}{\bar{S}} \geq \frac{M_{1,\eta}-c_4}{\lambda_1 K_1 \gamma_1} \\ \frac{S_{\eta\delta}(\gamma_1,\gamma_2)}{\bar{S}} \geq \frac{M_{2,\delta}-c_4}{\lambda_2 K_2 \gamma_2}, \end{cases} \tag{20}$$

where γ_1, γ_2, c_4, K_1, K_2, λ_1, and λ_2 are derived as part of previous subsection. For MQAM, λ_1, λ_2 are given by Eq. (13), whereas for MPSK, we have $\lambda_1 = \lambda_2 = 1$.

The most important difference between our discrete-rate and continuous-rate schemes is that in the discrete-rate scheme, the inequalities in Eq. (20) cannot assume equality at the same time. Since the rates only have discrete values, therefore a fixed $S_{\eta\delta}(\gamma_1, \gamma_2)$ cannot satisfy both equations simultaneously, except when $\gamma_1 = \gamma_2$, which is practically impossible in time-varying fading channels. Similarly to the single-user variable-rate, variable-power MQAM scheme discussed in [15], our proposed discrete-rate scheme cannot achieve the optimal performance of the continuous-rate adaptive scheme to be studied in Subsection C, hence there is an inevitable power-loss or rate-loss. Let us now continue by making some reasonable adjustments to our power control policy. Let

$$\frac{S_{\eta\delta}(\gamma_1, \gamma_2)}{\bar{S}} = \max\left\{\frac{M_{1,\eta} - c_4}{\lambda_1 K_1 \gamma_1}, \frac{M_{2,\delta} - c_4}{\lambda_2 K_2 \gamma_2}, 0\right\}, \tag{21}$$

where we have

$$\begin{cases} \lambda_1 = 1, \lambda_2 = \frac{1-M_{2,\delta}^{-1}}{1-M_{1,\eta}^{-1}}, \ if\ M_{1,\eta} \geq M_{2,\delta} \geq 2 \\ \lambda_1 = \frac{1-M_{1,\eta}^{-1}}{1-M_{2,\delta}^{-1}}, \lambda_2 = 1, \ if\ M_{2,\delta} \geq M_{1,\eta} \geq 2 \\ \lambda_1 = 1, \lambda_2 = 1, \ NC-PSK scheme. \end{cases} \tag{22}$$

Of particular note is that in Eq. (22), the constellation sizes are discrete, with their domains being $\{2, 4, 8, 16, \ldots\}$. Considering QAM for example, the constellation size is generally larger than 2 (corresponding to PAM).

According to Eq. (17), the optimization problem can be distilled down to maximizing

$$\frac{R}{B} = \sum_{\eta=0}^{N_1-1} \sum_{\delta=0}^{N_2-1} (\omega_1 \lambda_1 k_{1,\eta} + \omega_2 \lambda_2 k_{2,\delta}) \int\int_{D_{\eta,\delta}} p(\gamma_1) p(\gamma_2) d\gamma_1 d\gamma_2 \tag{23}$$

subject to

$$\begin{cases} \sum_{\eta=0}^{N_1-1} \sum_{\delta=0}^{N_2-1} \int\int_{D_{\eta,\delta}} \frac{S_{\eta\delta}(\gamma_1,\gamma_2)}{\bar{S}} p(\gamma_1) p(\gamma_2) d\gamma_1 d\gamma_2 = 1 \\ D_{\eta,\delta} \bigcap D_{\eta',\delta'} = \phi \\ \bigcup_\eta \bigcup_\delta D_{\eta,\delta} = \mathbb{R}^2, \end{cases} \tag{24}$$

where $D_{\eta,\delta}$ and $D_{\eta',\delta'}$ denote the different regions corresponding to the different transmit rates of $k_{1,\eta}$, $k_{2,\delta}$ and $k_{1,\eta'}$, $k_{2,\delta'}$.

To find the optimal fading-magnitude divisions for each destination node, we may also formulate the Lagrangian with the aid of the KKT conditions. However, the shape of $D_{\eta,\delta}$ obeys arbitrary quadrilaterals, therefore the discrete-rate optimization problem becomes excessively complex to be solved with the aid of general optimization methods. Inspired by the basic set-partition algorithm of [15], without changing the nature of the problem, we make some adjustments for our problem by restricting the fading-magnitude regions into rectangular areas (Fig. 3 shows the schematic of this version). In each rectangular area, we use the constellation sizes $M_{1,\eta}, \eta \in \mathbb{N}$ for DN1 and $M_{1,\delta}, \delta \in \mathbb{N}$ for DN2, which determine the attainable transmission rates.

$$\begin{aligned} J[\upsilon^*, D, \gamma_1, \gamma_2, S(\gamma_1, \gamma_2)] = &\int\int_D R[\gamma_1, \gamma_2, S(\gamma_1, \gamma_2)]\, d\gamma_1 d\gamma_2 + \upsilon^* \left(\bar{S} - \int\int_D S(\gamma_1, \gamma_2) p(\gamma_1) p(\gamma_2) d\gamma_1 d\gamma_2\right) \\ &+ \int\int_D \mu^* S(\gamma_1, \gamma_2) p(\gamma_1) p(\gamma_2) d\gamma_1 d\gamma_2 \end{aligned} \tag{18}$$

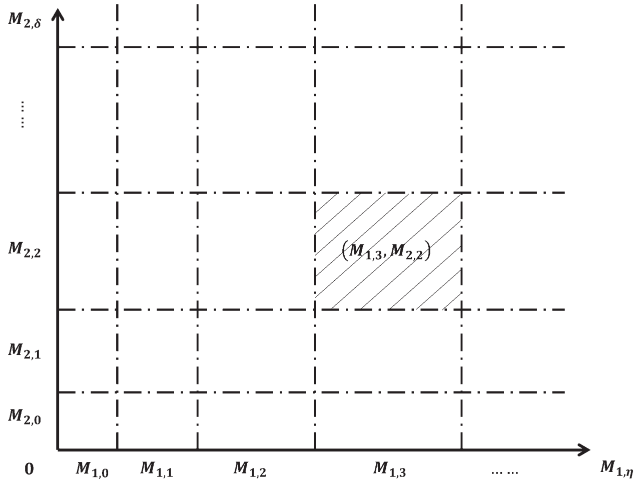

Fig. 3. Schematic of rectangular areas.

According to our adjusted method, the optimization problem can be simplified to that of maximizing

$$\frac{R}{B}=\sum_{\eta=0}^{N_1-1}\sum_{\delta=0}^{N_2-1}(\omega_1 k_{1,\eta}+\omega_2 k_{2,\delta})\int_{\gamma_{1,\eta-1}}^{\gamma_{1,\eta}} p(\gamma_1)d\gamma_1 \int_{\gamma_{2,\delta-1}}^{\gamma_{2,\delta}} p(\gamma_2)d\gamma_2 \tag{25}$$

subject to

$$\begin{cases} \sum_{\eta=0}^{N_1-1}\sum_{\delta=0}^{N_2-1}\int_{\gamma_{1,\eta-1}}^{\gamma_{1,\eta}}\int_{\gamma_{2,\delta-1}}^{\gamma_{2,\delta}} \frac{S_{\eta\delta}(\gamma_1,\gamma_2)}{S} p(\gamma_1)p(\gamma_2)d\gamma_1 d\gamma_2 = 1 \\ 0<\gamma_{1,0}<\ldots<\gamma_{1,\eta-1}<\gamma_{1,\eta}<\ldots<\gamma_{1,N_1-1} \\ 0<\gamma_{2,0}<\ldots<\gamma_{2,\delta-1}<\gamma_{2,\delta}<\ldots<\gamma_{2,N_2-1}, \end{cases} \tag{26}$$

where $\gamma_{1,\eta}$ and $\gamma_{1,j}$ denote the rectangular fading region boundaries, and again, $k_{1,\eta}$, $k_{2,\delta}$, $p(\gamma_1)$, $p(\gamma_2)$, ω_1 and ω_2 are derived previously.

The corresponding power adaptation policy is the same as that of Eq. (21). Upon substituting Eq. (21) into Eq. (26), we may rewrite the power constraint as Eq. (27), shown at the bottom of the page. An intuitive interpretation of Eq. (27) is as follows. Throughout the entire fading-magnitude region, given γ_1, γ_2 and $S_{\eta\delta}(\gamma_1,\gamma_2)$, the discrete transmit rates destined for DN1 and DN2 cannot reach their optimal match with the same power at the same time. However, in the context of joint optimization, Eq. (21) facilitates that at least one of the equalities is satisfied in Eq. (20), which implies that if one of the user's rate and power achieves the optimal match,[2] the other user will have a rate determined by the maximum constellation size it can reach. In other words, it is highly likely that for the other DL user, the power will be higher than that required by the user's modulation mode at this moment. Intuitively, according to our proposed power allocation policy, the optimization target is that of maximizing the pair of users' weighted sum rate. Therefore, the index of the particular user that reaches its optimal match with the available power depends mainly on its weight coefficient and instantaneous SNR. In other words, the identifier of the specific user that reaches its optimal power and rate match is ultimately determined by its contribution to the sum rate.

Based on the above discussions, we may obtain the optimal region partitions $R_{1,\eta}=[\gamma_{1,\eta-1},\gamma_{1,\eta})$, $\eta=0,\ldots,N_1-1$ and $R_{2,\delta}=[\gamma_{2,\delta-1},\gamma_{2,\delta})$, $\delta=0,\ldots,N_2-1$, which are jointly determined by the average power constraint and the fading distributions. There is no closed-form solution to this kind of problem [15]. However, similarly to the approach of [15], we conceive a numerical search algorithm *with low complexity* for finding the optimal boundaries[3] $R_{1,\eta}$ and $R_{2,\delta}$. This may require a large amount of calculations. However, once the optimal boundaries have been found, they can be used without real-time calculations.

C. Continuous-Rate Adaptive M-ary NC-QAM/PSK

According to the optimization problem formulated in Subsection A, our continuous-rate adaptive NC-QAM and the concept of generalized adaptive NCM will be investigated in this subsection. In contrast to the information theoretic discussion of [18], the proposed continuous-rate adaptive NCM schemes are based on BER bounds. More particularly, the SNR-loss imposed by adaptive NC-QAM will be discussed in the context of the associated BER expressions. For PSK and other M-ary modulations, which obey the BER-bound of (11), a unified solution is presented, which relies on channel prediction.

1) Continuous-Rate Adaptation for NC-QAM: As discussed in Subsection A, a tight BER bound is given by Eq. (11). For NC-QAM, the maximum constellation size capable of meeting the target P_{b_i} is given by Eq. (14). Let $c_1=0.2$, $c_2=1.5$, $c_3=1$ and $c_4=1$ when $M_i \geq 4$ and $0 \leq \gamma_i \leq 30$ dB [23]. For our continuous-rate scheme, the pair of inequalities in Eq. (14) are capable of simultaneously meeting the equality conditions. We then have

$$\begin{cases} M_1(\gamma_1) = 1 + K_1\lambda_1\gamma_1 \frac{S(\gamma_1,\gamma_2)}{\bar{S}} \\ M_2(\gamma_2) = 1 + K_2\lambda_2\gamma_2 \frac{S(\gamma_1,\gamma_2)}{\bar{S}}, \end{cases} \tag{28}$$

where $K_i = -1.5/\ln(5P_{b_i})$, $i=1,2$.

According to Eq. (16), the rate function of jointly-optimal NC-QAM may be formulated as

$$R\left[\gamma_i, S(\gamma_1,\gamma_2)\right]=\sum_{i=1}^{2}\omega_i \log_2\left(1+K_i\lambda_i\gamma_i\frac{S(\gamma_1,\gamma_2)}{\bar{S}}\right),\ i=1,2. \tag{29}$$

[2]Here, the optimal match implies that the transmit power is the one which happens to be the power that a specific modulation mode requires.

[3]The optimal boundaries are the optimal channel state thresholds corresponding to the different modulation modes.

$$\sum_{\eta=0}^{N_1-1}\sum_{\delta=0}^{N_2-1}\int_{\gamma_{1,\eta-1}}^{\gamma_{1,\eta}}\int_{\gamma_{2,\delta-1}}^{\gamma_{2,\delta}} \max\left\{\frac{M_{1,\eta}-c_4}{\lambda_1 K_1\gamma_1}, \frac{M_{2,\delta}-c_4}{\lambda_2 K_2\gamma_2}, 0\right\} p(\gamma_1)p(\gamma_2)d\gamma_1 d\gamma_2 = 1 \tag{27}$$

Again, the SNR-loss imposed by NC-QAM was quantified in terms of a so-called 'SNR-loss coefficient λ' in [8], which will now be considered in the context of Eq. (13). Specifically, we found that for the larger constellation size of the two, there is no SNR-loss according to [8]. In other words, the SNR loss only exists for the specific destination node, which has the smaller constellation size. Furthermore, the SNR-loss decreases upon increasing the receiver-side SNR. Based on the above discussions, we treat the coefficients λ_1 and λ_2 as a pair of inequality constrains.

For fading channels, we substitute Eq. (29) into Eq. (17) and then reformulate the optimization problem by maximizing

$$\frac{R}{B}=\int_0^\infty\int_0^\infty\sum_{i=1}^{2}\omega_i \log_2\left(1+K_i\lambda_i\gamma_i\frac{S(\gamma_1,\gamma_2)}{\bar{S}}\right)p(\gamma_1)p(\gamma_2)d\gamma_1 d\gamma_2 \tag{30}$$

subject to

$$\begin{cases} \int_0^\infty\int_0^\infty S(\gamma_1,\gamma_2)p(\gamma_1)p(\gamma_2)d\gamma_1 d\gamma_2=\bar{S} \\ S(\gamma_1,\gamma_2)\geq 0 \\ \lambda_1\left(1-\frac{1}{(1+K_2\gamma_2\lambda_2 S(\gamma_1,\gamma_2/\bar{S})}\right)\leq 1-\frac{1}{(1+K_1\gamma_1\lambda_1 S(\gamma_1,\gamma_2)/\bar{S})} \\ \lambda_2\left(1-\frac{1}{(1+K_1\gamma_1\lambda_1 S(\gamma_1,\gamma_2)/\bar{S})}\right)\leq 1-\frac{1}{(1+K_2\gamma_2\lambda_2 S(\gamma_1,\gamma_2)/\bar{S})} \\ \lambda_1\leq 1 \\ \lambda_2\leq 1, \end{cases} \tag{31}$$

$$\lambda_i=\min\left(1,\frac{1-M_i(\gamma_i)^{-1}}{1-M_{3-i}(\gamma_{3-i})^{-1}}\right),\quad i=1,2, \tag{32}$$

where ω_1, ω_2, $\bar{S}$, $S(\gamma_1,\gamma_2)$, γ_i, $\overline{\gamma_i}$, $p(\gamma_i)$ and P_{b_i} are defined as in the previous subsection.

Upon substituting Eq. (32) into Eq. (30), we arrive at a challenging problem, which is difficult to solve using general mathematical tools. When considering the SNR-loss coefficients, we will simplify our discussions by setting an upper bound and a lower bound for λ_i.

The upper bound readily emerges by letting $\lambda_1=\lambda_2=1$, which means that there is no SNR-loss. As to the lower bound, we first set $\lambda_1=\lambda_2=\lambda^*$, which results in:

$$\begin{cases} M_1(\gamma_1)=1+K_1\lambda^*\gamma_1\frac{S(\gamma_1,\gamma_2)}{\bar{S}} \\ M_2(\gamma_2)=1+K_2\lambda^*\gamma_2\frac{S(\gamma_1,\gamma_2)}{\bar{S}}. \end{cases} \tag{33}$$

We now have to discuss different cases for Eq. (33). If we consider $K_1\gamma_1\geq K_2\gamma_2$ first, then we have $M_1(\gamma_1)\geq M_2(\gamma_2)$. According to Eq. (13), the SNR-loss coefficients λ^* now becomes

$$\begin{aligned}\lambda^*&=\frac{1-\left(1+K_2\lambda^*\gamma_2\frac{S(\gamma_1,\gamma_2)}{\bar{S}}\right)^{-1}}{1-\left(1+K_1\lambda^*\gamma_1\frac{S(\gamma_1,\gamma_2)}{\bar{S}}\right)^{-1}}\\ &>1-\left(1+K_2\lambda^*\gamma_2\frac{S(\gamma_1,\gamma_2)}{\bar{S}}\right)^{-1}.\end{aligned} \tag{34}$$

Since the constellation size of MQAM is larger than 2, we then set the lower bound by letting $M_1(\gamma_1)\geq M_2(\gamma_2)\geq 2$, which implies that we may have

$$\lambda^*>1-\left(1+K_2\lambda^*\gamma_2\frac{S(\gamma_1,\gamma_2)}{\bar{S}}\right)^{-1}=\frac{1}{2}. \tag{35}$$

For the scenario of $K_1\gamma_1\leq K_2\gamma_2$, we may get result similar to Eq. (35). Since the SNR-loss decreases upon increasing the constellation size, it is reasonable to set a lower bound by letting $\lambda^*=0.5$. Hence we have found both a lower and an upper bound for the SNR-loss coefficients.

Let us now discuss the corresponding solutions for adaptive NC-QAM. Let us commence by considering the simple case of $\lambda_1=\lambda_2=1$, for the target BER functions associated with $K_1=K_2=K$ and the weight factors of $\omega_1=\omega_2=0.5$. To find the optimal power allocation $S(\gamma_1,\gamma_2)$, we substitute $\lambda_1=\lambda_2=1$, as well as $K_1=K_2=K$ into Eq. (30) and Eq. (31). Then we may rewrite Eq. (18) as

$$\begin{aligned} &J\left[S(\gamma_1,\gamma_2)\right]\\ &=\int_0^\infty\int_0^\infty\sum_{i=1}^{2}\omega_i\log_2\left(1+K\gamma_i\frac{S(\gamma_1,\gamma_2)}{\bar{S}}\right)p(\gamma_1)p(\gamma_2)d\gamma_1 d\gamma_2\\ &\quad+\upsilon^*\left(\bar{S}-\int_0^\infty\int_0^\infty S(\gamma_1,\gamma_2)p(\gamma_1)p(\gamma_2)d\gamma_1 d\gamma_2\right)\\ &\quad+\int_0^\infty\int_0^\infty \mu^* S(\gamma_1,\gamma_2)p(\gamma_1)p(\gamma_2)d\gamma_1 d\gamma_2. \end{aligned} \tag{36}$$

Upon differentiating the Lagrangian and setting the resultant derivative to zero, we arrive at:

$$\frac{\partial J\left[S(\gamma_1,\gamma_2)\right]}{\partial S(\gamma_1,\gamma_2)}=0,\ \frac{\partial J(\upsilon^*)}{\partial \upsilon^*}=0, \tag{37}$$

yielding:

$$\begin{cases} \left[\sum_{i=1}^2\omega_i\left(\frac{1/\ln 2}{1+K\gamma_i\frac{S(\gamma_1,\gamma_2)}{\bar{S}}}\right)\frac{K\gamma_i}{\bar{S}}-\upsilon^*+\mu^*\right]p(\gamma_1)p(\gamma_2)=0 \\ \mu^* S(\gamma_1,\gamma_2)=0 \\ S(\gamma_1,\gamma_2)\geq 0 \\ \mu^*\geq 0. \end{cases} \tag{38}$$

Solving Eq. (38) for $S(\gamma_1,\gamma_2)$ under the relevant power constraint yields the complementary slack condition υ^* (see bottom of the next page)[4] and the power adaptation policy that maximizes Eq. (30), as seen in Eq. (39), shown at the bottom of the next page. Upon substituting the channel estimates and the power adaptation policy of Eq. (39) back into Eq. (30), we arrive at the jointly-optimized cutoff fade depth υ^*, below which the transmissions are disabled. Then the maximum spectral efficiency can be achieved for the parameters γ_1, γ_2, $p(\gamma_1)$,

[4]Firstly, when $\mu^*>0, S(\gamma_1,\gamma_2)=0$, we have $(\omega_1 K\gamma_1/\overline{S}\ln 2)+(\omega_2 K\gamma_2/\overline{S}\ln 2)-\upsilon^*+\mu^*=0\Rightarrow\upsilon^*>(\omega_1 K\gamma_1+\omega_2 K\gamma_2/\overline{S}\ln 2)$. Secondly, when $\mu^*=0, S(\gamma_1,\gamma_2)>0$, we have $\upsilon^*=(\omega_1 K\gamma_1/\overline{S}\ln 2(1+K\gamma_1(S(\gamma_1,\gamma_2)/\overline{S})))+(\omega_2 K\gamma_2/\overline{S}\ln 2(1+K\gamma_2(S(\gamma_1,\gamma_2)/\overline{S})))<(\omega_1 K\gamma_1+\omega_2 K\gamma_2/\overline{S}\ln 2)$. Finally, the critical value is classified into the first case. So we get the complementary slack condition υ^*.

$p(\gamma_2)$, ω_1, ω_2, P_{b_1} and P_{b_2}. For the lower bound of $\lambda_i = 0.5$, we may arrive at a similar expression.

What has been discussed above is a special case of MQAM, where the BER requirements at both DN1 and DN2 are the same and the SNR loss coefficients are $\lambda_i = 1$. In the following subsection we will extend our variable-rate, variable-power adaptation scheme to more general schemes, such as NC-PSK, where there is no SNR loss.

2) Continuous-Rate Adaptation for General M-ary Modulation: The variable-rate and variable-power techniques discussed above for MQAM can be applied to other M-ary modulations. For any modulation scheme having a BER expression similar to Eq. (11), the basic premises are the same. Both the transmit power and the constellation sizes are adapted for maintaining both target BERs of the DN1 and DN2, while maximizing the overall rates. Given the parameters of $\bar{S}$, $S(\gamma_1,\gamma_2)$, γ_i, $\overline{\gamma_i}$, $p(\gamma_i)$ and P_{b_i} in our system model, there is no SNR-loss in the BER expression of NC-PSK, therefore we let $\lambda_1 = \lambda_2 = 1$ for our adaptive NC-PSK scheme. Without loss of generality, the BER requirements of NC-PSK can be different, given K_1 and K_2 in Eq. (15). Using the same method as in the previous subsection, we arrive at the following more general power adaptation policy see Eq. (40), shown at the bottom of the page.

When considering MPSK relying on the BER bound of Eq. (9.49) in [23] for example, by substituting $c_1 = 0.05$, $c_2 = 6$, $c_3 = 1.9$, $c_4 = 1$, γ_i, $\overline{\gamma_i}$, $p(\gamma_i)$ and P_{b_i} into Eq. (15), we may find the best cutoff fade depth υ^*, which hence allows us to calculate the maximum achievable spectral efficiency for the conditions considered.

D. Continuous-Rate Discretization for Adaptive M-ary QAM/PSK

Based on our discussions of the continuous-rate adaptation scheme of Subsection C, in this subsection, we proposed another discrete-rate transmission scheme, which we refer to as the Continuous-Rate Discretization Algorithm of NC-QAM/PSK. In our following discussions we consider the SNR loss upper bound of $\lambda_1 = \lambda_2 = 1$ for MQAM.

We assume that the parameters of our continuous-rate scheme have already been calculated. The divisions of the fading-magnitude regions are the same as in Subsection B. The discrete sets of MQAM/MPSK transmission modes are $\mathcal{M}_1 = \{M_{1,0}, \ldots, M_{1,N_1-1}\}$, $\mathcal{M}_2 = \{M_{2,0}, \ldots, M_{2,N_2-1}\}$, with $M_{1,0} = 0$ and $M_{2,0} = 0$ implying no transmission. Let $M'_{1,\eta}$ and $M'_{2,\delta}$ denote the new rates corresponding to the continuous rates of M_1 and M_2, when they falls into specific fading-partitions. According to Eq. (17), the target problem now becomes that of calculating Eq. (41), shown at the bottom of the page, where $M'_{1,\eta}$ and $M'_{2,\delta}$ are obtained with the aid of Algorithm 1. Again, $\omega_1, \omega_2, \gamma_1, \gamma_2, p(\gamma_1), p(\gamma_2), P_{b_1}, P_{b_2}$ and $\overline{S}$ are all the same, as in the previous subsections.

Algorithm 1 Continuous Rate Discretization Algorithm

Step 1) Calculate the corresponding parameters M_1, M_2, $S(\gamma_1,\gamma_2)$ and υ^* for given γ_1, γ_2 values in the context of our continuous-rate adaptive scheme.

Step 2) Round M_1, M_2 down to the nearest integer constellation sizes of $M'_{1,\eta} \in \mathcal{M}_1, M'_{2,\delta} \in \mathcal{M}_2$ with $S(\gamma_1,\gamma_2)$ remaining unchanged.

Step 3) Substitute $M'_{1,\eta}$, $M'_{2,\delta}$ into Eq. (41) and recalculate the spectral efficiency.

It is important to note that when we round the continuous-valued M_1, M_2 down to the nearest integers, the transmit power $S(\gamma_1,\gamma_2)$ remains unchanged. Additionally, letting $\lambda_1 = \lambda_2 = 1$ for MQAM implies that we ignore the SNR loss, which is indeed small enough to be neglected. Although this arrangement is not as beneficial as the scheme of Subsection B, the proposed design provides another feasible technique of realizing adaptive NC-QAM/PSK.

$$\frac{S(\gamma_1,\gamma_2)}{\bar{S}} = \begin{cases} \frac{1}{2}\sqrt{\left(\frac{1}{K\gamma_1}+\frac{1}{K\gamma_2}-\frac{1}{\upsilon^*\bar{S}\ln 2}\right)^2 - \frac{4}{\upsilon^* K^2\gamma_1\gamma_2}\left(\upsilon^* - \frac{\omega_1 K\gamma_1+\omega_2 K\gamma_2}{\bar{S}\ln 2}\right)} + \frac{1}{2\upsilon^*\bar{S}\ln 2} - \frac{1}{2K\gamma_1} - \frac{1}{2K\gamma_2}, \upsilon^* < \frac{\omega_1 K\gamma_1+\omega_2 K\gamma_2}{\bar{S}\ln 2} \\ 0, \upsilon^* \geq \frac{\omega_1 K\gamma_1+\omega_2 K\gamma_2}{\bar{S}\ln 2} \end{cases} \tag{39}$$

$$\frac{S(\gamma_1,\gamma_2)}{\bar{S}} = \begin{cases} \frac{1}{2}\sqrt{\left(\frac{c_4}{K_1\gamma_1}+\frac{c_4}{K_2\gamma_2}-\frac{1}{\upsilon^* c_3\bar{S}\ln 2}\right)^2 - \frac{4}{\upsilon^* K_1K_2\gamma_1\gamma_2}\left(\upsilon^* c_4^2 - \frac{\omega_1 c_4 K_1\gamma_1+\omega_2 c_4 K_2\gamma_2}{c_3\bar{S}\ln 2}\right)} + \frac{1}{2\upsilon^* c_3\bar{S}\ln 2} - \frac{c_4}{2K_1\gamma_1} - \frac{c_4}{2K_2\gamma_2}, \\ \upsilon^* < \frac{\omega_1 K_1\gamma_1+\omega_2 K_2\gamma_2}{c_3 c_4\bar{S}\ln 2} \\ 0, \upsilon^* \geq \frac{\omega_1 K_1\gamma_1+\omega_2 K_2\gamma_2}{c_3 c_4\bar{S}\ln 2} \end{cases} \tag{40}$$

$$\frac{R}{B} = \int_0^\infty \int_0^\infty \sum_{\eta=1}^{N_1-1} \sum_{\delta=1}^{N_2-1} \left[\frac{\omega_1}{c_3}\log_2\left(M'_{1,\eta}\right) + \frac{\omega_2}{c_3}\log_2\left(M'_{2,\delta}\right)\right] p(\gamma_1)p(\gamma_2)d\gamma_1 d\gamma_2 \tag{41}$$

TABLE I
SCENARIOS AND UNIFIED PARAMETERS FOR QAM

Scenarios	Rate and Power Strategies	System Model	Bound	BER	SNR loss	Unified Parameters
Scenario 1	AWGN Channel Capacity					
Scenario 2	Optimal Rate and Power Adaptation	Single-User	Shannon Bound			$p(\gamma_i) = \frac{1}{\overline{\gamma_i}} e^{-\gamma_i/\overline{\gamma_i}}, i = 1, 2.$
Scenario 3	Optimal Rate and Power Adaptation	DF-TWR				$\overline{S} = 1$
Scenario 4	Optimal Rate and Constant Power	Single-User				$B = 1$
Scenario 5	Optimal Rate and Power Adaptive MQAM	Single-User	BER Bound	P_b=10^{-3}		$\omega_1 = \omega_2 = 0.5$
Scenario 6	Optimal Rate and Power Adaptive M-ary NC-QAM	DF-TWR		P_{b_1}=P_{b_2}=10^{-3}	λ_1=λ_2=1	$\gamma_i \in [0, 10 * \overline{\gamma_i}]\,, i = 1, 2$
Scenario 7	Optimal Rate and Power Adaptive M-ary NC-QAM	DF-TWR		P_{b_1}=P_{b_2}=10^{-3}	λ_1=λ_2=0.5	$\overline{\gamma_i}$={ 1,2,3,4,5,10,15,30,100,200,316}
Scenario 8	Optimal Rate and Constant Power	Single-User		P_b=10^{-3}		

TABLE II
SCENARIOS AND UNIFIED PARAMETERS FOR PSK

Scenarios	Rate and Power Strategies	System Model	Bound	BER	SNR loss	Unified Parameters
Scenario 1	AWGN Channel Capacity					
Scenario 2	Optimal Rate and Power Adaptation	Single-User	Shannon Bound			$p(\gamma_i) = \frac{1}{\overline{\gamma_i}} e^{-\gamma_i/\overline{\gamma_i}}, i = 1, 2.$
Scenario 3	Optimal Rate and Power Adaptation	DF-TWR				$\overline{S} = 1,\ B = 1$
Scenario 4	Optimal Rate and Constant Power	Single-User				$\omega_1 = \omega_2 = 0.5$
Scenario 5	Optimal Rate and Power Adaptive MPSK	Single-User	BER Bound	P_b=10^{-3}		$\gamma_i \in [0, 10 * \overline{\gamma_i}]\,, i = 1, 2$
Scenario 6	Optimal Rate and Power Adaptive M-ary NC-PSK	DF-TWR		P_{b_1}=P_{b_2}=10^{-3}		$\overline{\gamma_i}$= {1,2,3,4,5,10,15,30,100,200,316}
Scenario 7	Optimal Rate and Constant Power	Single-User		P_b=10^{-3}		

IV. PERFORMANCE RESULTS

A basic fixed-rate of NC-QAM/PSK was proposed in [8], [9], which provides the basis of our adaptive transmission scheme. In this section, a range of representative numerical results are presented for validating our theoretical analysis. Our emphasis is on the spectral efficiency of variable-rate, variable-power NC-QAM/PSK. Furthermore, both the continuous-rate and discrete-rate adaptive NC-QAM/PSK schemes are compared to their respective benchmark schemes for demonstrating its potential. Specifically, we invoke the single-user adaptive MQAM/MPSK scheme of [15], [23] and the Shannon capacity based joint-optimization schemes [14], [18] as our benchmarks, which are described as Scenario 1–8 in Tables I and II.

The following assumptions will be exploited throughout our simulations. Let us focus our attention on Rayleigh fading channels, where the fading distributions are given by Eq. (10). The near-instantaneous SNR fluctuations are limited to a dynamic range, which was set to be 10 times the average SNR. The SNR-loss coefficient upper bounds of NC-QAM are set to $\lambda_1 = \lambda_2 = 1$ (Scenario 6), while the lower bounds are set to $\lambda_1 = \lambda_2 = 0.5$ (Scenario 7). For continuous-rate adaptive NC-QAM/PSK schemes, all the other parameters of Scenarios 1–8 are depicted in Tables I and II.

Figs. 4 and 5 also include the benchmarks of [14] (versus Scenarios 4 and 8), [15] (versus Scenarios 2 and 5), [18] (versus Scenario 3), as well as Eqs. (39) and (40) (versus Scenarios 6 or 7) derived for our MQAM/MPSK scheme as a function of the average received SNR for transmission over Rayleigh fading channels. The capacity of an AWGN channel (versus Scenario 1) is also shown as comparison for the same average power. Several observations are worth discussing. Firstly, our adaptive NC-QAM/PSK is capable of approaching both the capacities of our proposed continuous-rate adaptive schemes, as well as of the schemes proposed in [18] and those of the single-user adaptation proposed in [15]. This is quite valuable, because we are supporting a bidirectional network-coded scenario.

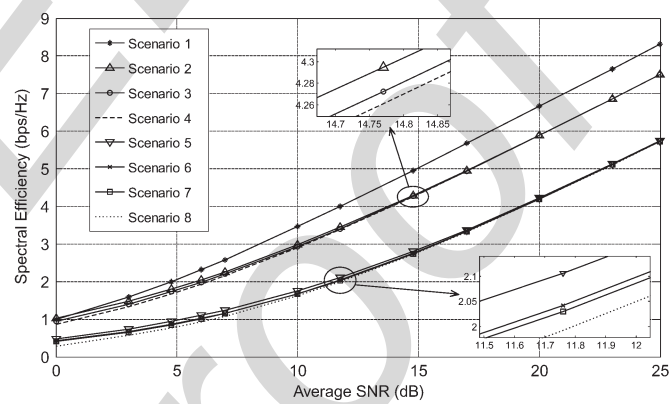

Fig. 4. Comparison of Scenarios 1–8 in terms of their spectral efficiency (QAM).

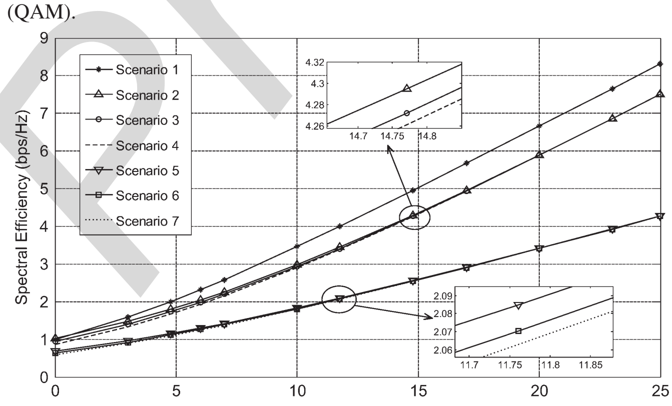

Fig. 5. Comparison of Scenarios 1–7 in terms of their spectral efficiency (PSK).

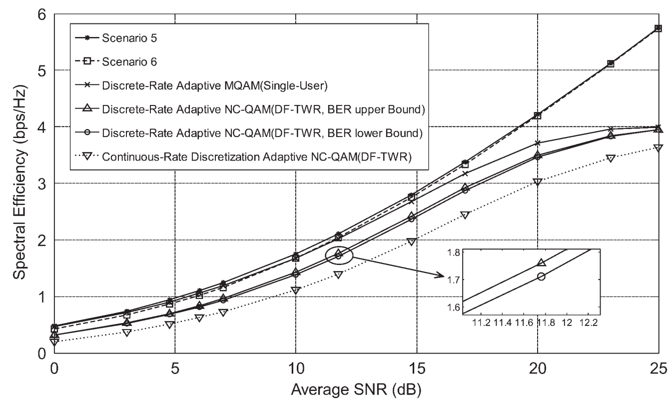

Fig. 6. Spectral efficiency of our continuous-rate adaptive NC-QAM, discrete-rate adaptive NC-QAM, continuous-rate discretization adaptive NC-QAM (Scenario 5, 6 of Fig. 4, $M = \{0, 2, 4, 16\}$).

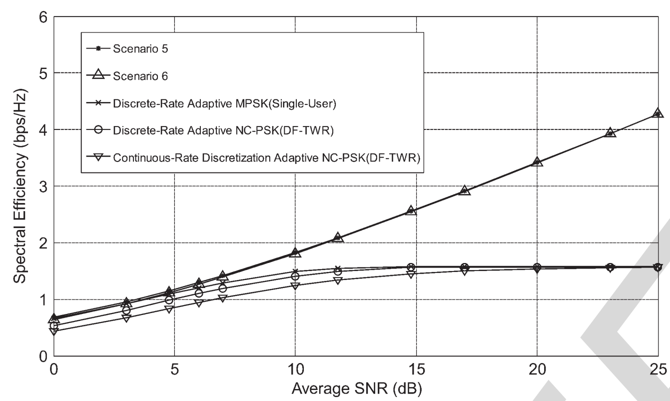

Fig. 7. Spectral efficiency of our continuous-rate adaptive NC-PSK, discrete-rate adaptive NC-PSK, continuous-rate discretization adaptive NC-PSK (Scenario 5, 6 of Fig. 5, $M = \{0, 2, 4, 8\}$).

Of particular note is in Fig. 4 that Eq. (39) relies on the upper bound of the SNR-loss coefficients, which were discussed in Section III. In Fig. 4 we also characterized NC-QAM relying on the SNR-loss lower bound associated with $\lambda_1 = \lambda_2 = 0.5$. The upper- and lower-bound curves are quite close to each other, which indicates that the impact of SNR-loss on the achievable spectral efficiency is small enough to be neglected. Secondly, both our schemes and the scheme proposed in [18] perform better than MQAM operating without power adaptation (versus Scenarios 8 and 7 in Figs. 4 and 5, respectively). Finally, upon increasing of the SNR, the discrepancy between our proposed schemes and the single-user adaptive schemes of [15] tends to narrow.

The continuous-rate discretization algorithm is now compared to the discrete-rate scheme proposed in Section III-B, using the same parameters of $\overline{\gamma_i} = [1, 2, 3, 4, 5, 10, 15, 30, 50, 100, 200, 316]$, $i = 1, 2$, $\gamma_i \in [0, 10 * \overline{\gamma_i}]$, $\overline{S} = 1$, $\omega = 0.5$, $P_{b_i} = 10^{-3}$, $B = 1$, and the Rayleigh distribution $p(\gamma_i)$ given by Eq. (10). We divide the dynamic range of the fading into four regions, and employ $\mathcal{M}_i = \{0, 2, 4, 16\}, i = 1, 2$ for MQAM and $\mathcal{M}_i = \{0, 2, 4, 8\}$, $i = 1, 2$ for MPSK. The SNR-loss parameters λ_i are given by Eq. (22) for MQAM and $\lambda_i = 1$ for MPSK.

Figs. 6 and 7 characterize the performance of our discrete-rate variable-power MQAM/MPSK scheme as well as of the adaptive single-user scheme of [15] (versus Scenario 5) and of the continuous-rate discretization algorithm of Section III-D. Both

TABLE III
RATE AND POWER ADAPTATION FOR MQAM (4 REGIONS)

$\gamma_{1,\eta}Range$	$\gamma_{2,\delta}Range$	M_1	M_2	$S_{\eta\delta}(\gamma_1, \gamma_2)/\overline{S}$
$0 \le \gamma_1 \le 1.3$	$0 \le \gamma_2 \le 1.3$	0	0	0
	$1.3 \le \gamma_2 \le 3.2$	0	2	$\max\{0, \frac{1}{K\gamma_2}\}$
	$3.2 \le \gamma_2 \le 6.0$	0	4	$\max\{0, \frac{3}{K\gamma_2}\}$
	$6.0 \le \gamma_2 \le 10$	0	16	$\max\{0, \frac{7}{K\gamma_2}\}$
$1.3 \le \gamma_1 \le 3.2$	$0 \le \gamma_2 \le 1.3$	2	0	$\max\{\frac{1}{K\gamma_1}, 0\}$
	$1.3 \le \gamma_2 \le 3.2$	2	2	$\max\{\frac{1}{K\gamma_1}, \frac{1}{K\gamma_2}\}$
	$3.2 \le \gamma_2 \le 6.0$	2	4	$\max\{\frac{1}{(2/3)K\gamma_1}, \frac{3}{K\gamma_2}\}$
	$6.0 \le \gamma_2 \le 10$	2	16	$\max\{\frac{1}{(8/15)K\gamma_1}, \frac{15}{K\gamma_2}\}$
...	...	...	...	...
$6.0 \le \gamma_1 \le 10$	$3.2 \le \gamma_2 \le 6.0$	16	4	$\max\{\frac{15}{K\gamma_1}, \frac{3}{(4/5)K\gamma_2}\}$
$6.0 \le \gamma_1 \le 10$	$6.0 \le \gamma_2 \le 10$	16	16	$\max\{\frac{15}{K\gamma_1}, \frac{15}{K\gamma_2}\}$

TABLE IV
RATE AND POWER ADAPTATION FOR MPSK (4 REGIONS)

$\gamma_{1,\eta}Range$	$\gamma_{2,\delta}Range$	M_1	M_2	$S_{\eta\delta}(\gamma_1, \gamma_2)/\overline{S}$
$0 \le \gamma_1 \le 0.5$	$0 \le \gamma_2 \le 0.5$	0	0	0
	$0.5 \le \gamma_2 \le 1.1$	0	2	$\max\{0, \frac{1}{K\gamma_2}\}$
	$1.1 \le \gamma_2 \le 2.5$	0	4	$\max\{0, \frac{3}{K\gamma_2}\}$
	$2.5 \le \gamma_2 \le 10$	0	8	$\max\{0, \frac{7}{K\gamma_2}\}$
$0.5 \le \gamma_1 \le 1.1$	$0 \le \gamma_2 \le 0.5$	2	0	$\max\{\frac{1}{K\gamma_1}, 0\}$
	$0.5 \le \gamma_2 \le 1.1$	2	2	$\max\{\frac{1}{K\gamma_1}, \frac{1}{K\gamma_2}\}$
	$1.1 \le \gamma_2 \le 2.5$	2	4	$\max\{\frac{1}{K\gamma_1}, \frac{3}{K\gamma_2}\}$
	$2.5 \le \gamma_2 \le 10$	2	8	$\max\{\frac{1}{K\gamma_1}, \frac{7}{K\gamma_2}\}$
...	...	...	...	...
$2.5 \le \gamma_1 \le 10$	$1.1 \le \gamma_2 \le 2.5$	8	4	$\max\{\frac{7}{K\gamma_1}, \frac{7}{K\gamma_2}\}$
$2.5 \le \gamma_1 \le 10$	$2.5 \le \gamma_2 \le 10$	8	8	$\max\{\frac{7}{K\gamma_1}, \frac{7}{K\gamma_2}\}$

Figs. 6 and 7 show that the performance of our discrete-rate schemes approaches that of the adaptive single-user MQAM/MPSK schemes proposed in [15], despite the more challenging scenario of supporting bidirectional NC. According to Fig. 4, the proposed discrete-rate schemes exhibit a better performance than the scheme operating without power adaptation. Compared to the continuous-rate discretization algorithm, the discrete-rate continuous-power scheme proposed in Section III-B performs better. Additionally, it is important to note that in Fig. 6 we characterize the adaptive MQAM algorithm without considering the SNR-loss λ_i. Compared to adaptive MQAM taking into consideration the SNR-loss, the two curves are close, which indicates that the SNR-loss of the discrete-rate scheme is small enough to be ignored. Our simulation results also indicate that the gaps between our proposed schemes, the continuous-rate discretization algorithm and the adaptive single-user methods of [15] tend to decrease upon increasing of the average SNRs. Moreover, increasing the number N_i of discrete signal constellations yields a

TABLE V
PERFORMANCE COMPARISON OF CONTINUOUS-RATE AND DISCRETE-RATE SCHEMES (QAM)

Rate(bps/Hz)	$\overline{\gamma_i}$=1	$\overline{\gamma_i}$=2	$\overline{\gamma_i}$=3	$\overline{\gamma_i}$=4	$\overline{\gamma_i}$=5	$\overline{\gamma_i}$=10	$\overline{\gamma_i}$=15	$\overline{\gamma_i}$=30	$\overline{\gamma_i}$=50	$\overline{\gamma_i}$=100	$\overline{\gamma_i}$=200	$\overline{\gamma_i}$=316
Single-User Continuous Adaptation (Shannon bound)	0.4836	0.7421	0.9384	1.1012	1.2401	1.7519	2.1064	2.8005	3.3747	4.2215	5.1249	5.7434
DF-TWR Continuous Adaptation	0.4235	0.6702	0.8620	1.0226	1.1624	1.6804	2.0420	2.7517	3.3377	4.1978	5.1112	5.7338
Single-User Discrete-Rate Adaptive MQAM	0.4679	0.7158	0.9024	1.0558	1.1878	1.6786	2.0220	2.6809	3.1719	3.7060	3.9572	3.9951
DF-TWR Discrete-Rate Adaptive NC-QAM(SNR-loss upper bound)	0.3207	0.5281	0.6949	0.8375	0.9616	1.4274	1.7597	2.4193	2.9279	3.4989	3.8451	3.9526
DF-TWR Discrete-Rate Adaptive NC-QAM(SNR-loss lower bound)	0.3181	0.5210	0.6816	0.8171	0.9357	1.3857	1.7113	2.3606	2.8671	3.4587	3.8316	3.9485
Continuous-Rate Discretization Adaptive NC-QAM	0.1967	0.3667	0.5078	0.6275	0.7315	1.1149	1.3910	1.9717	2.4489	3.0335	3.4521	3.6356

better match with the continuous-rate adaptation scheme, hence resulting in a higher spectral efficiency.

Let us now conclude by considering both the power-allocation and rate-adaptation policy for a specific scenario, using the parameters of $\overline{\gamma_i} = 1, i = 1, 2, \gamma_i \in [0, 10], w_i = 0.5$, $P_{b_i} = 10^{-3}$, $\overline{S} = 1$, $B = 1$, $\mathcal{M}_i = \{0, 2, 4, 16\}$ for MQAM and $\mathcal{M}_i = \{0, 2, 4, 8\}$ for MPSK. The SNR-loss coefficients λ_i are given by Eq. (22) for MQAM and $\lambda_i = 1$ for MPSK.

In Table III we summarize the constellation sizes and power adaptation policies as functions of γ_1 and γ_2 for four fading regions corresponding to four MQAM/MPSK adaptive strategies. Upon solving Eqs. (25) and (27) we arrive at the corresponding switching thresholds divisions for MQAM as $R_1 = [0, 1.3, 3.2, 6.0, 10]$, $R_2 = [0, 1.3, 3.2, 6.0, 10]$, which are required for practical use. The corresponding maximum rate is 0.3207 bps/Hz. Similarly, Table IV characterizes the discrete-rate adaption scheme for MPSK under the same conditions as for MQAM, where we have $R_1 = [0, 0.5, 1.1, 2.5, 10]$, $R_2 = [0, 0.5, 1.1, 2.5, 10]$. The corresponding maximum rate is 0.5375 bps/Hz.

In Table V we tabulate the concrete numerical values of spectral efficiency for the Scenarios 1–8 of Fig. 6, which well support our conclusions.

V. CONCLUSION

In this paper, we developed an asymmetric adaptive transmission design for DF-TWR, which combines network coding with near-instantaneously adaptive modulation that adapts to the channel variations. The main emphasis of this design is on practical adaptive NCM, therefore our study was focused on discrete-rate adaptation schemes. Our simulation results demonstrated that the proposed variable-rate, variable-power NC-QAM/PSK DF-TWR schemes are capable of obtaining a higher spectral efficiency compared to the benchmark scheme operating without power adaptation. Finally, we demonstrated that the impact of SNR-loss on the achievable spectral efficiency is sufficiently low to be neglected.

APPENDIX
SNR-LOSS IMPOSED BY NC-QAM

For NC-QAM, the symbol to be transmitted to DN1 and DN2 will be circularly shifted by an amplitude of $2\sqrt{M_2}(a_i^I + ja_i^Q)d$ at the relay [8]. When we derive the symbol error rate (SER) of NC-QAM, intuitively, the SER of a circularly shifted M_i-ary QAM constellation is identical to that of the original M_i-ary QAM for the same minimum symbol distance. By recalling Eq. (3), Eq. (5) and that $a_i^I, a_i^Q \in \mathcal{A}_i$, we have $d_1 = (\sqrt{M_2}/\sqrt{M_1})d$ and $d_2 = d$. Let us insert d_1 and d_2 into Eq. (42) and introduce the M_1- and M_2-dependent coefficient of $\lambda_i = (1 - M_i^{-1}/1 - M_2^{-1}), M_2 > M_1$:

$$P_i = \frac{4(\sqrt{M_i} - 1)}{\sqrt{M_i}} Q\left(\sqrt{\frac{|h_i|^2 d_i^2}{N_0/2}}\right), \tag{42}$$

where P_i denotes the SER of the relay-DN1 and relay-DN2 links. We may thus arrive at the unified SER expressions of NC-QAM, given by

$$P_i = \frac{4(\sqrt{M_i} - 1)}{\sqrt{M_i}} Q\left(\sqrt{\frac{1.5\lambda_i \gamma_i}{M_i - 1}}\right). \tag{43}$$

According to the above analysis, for $M_2 > M_1$, we have $\lambda_1 = 1$ and $\lambda_2 < 1$, which implies imposing an SNR loss for the relay-DN1 link that remains constant across the entire SNR range. The reason for this SNR loss at the receiver of DN1 can be stated as follows. Since QAM is regarded as a pair of orthogonal signals PAM, we may simply focus our discussions on the I component. Given a_2^I, the legitimate symbols at the receiver of DN1 have a non-zero mean of

$$d\left[2\sqrt{M_2}\left(a_2^I \bmod \frac{1}{\sqrt{M_1}}\right) + 1 - \frac{\sqrt{M_2}}{\sqrt{M_1}}\right]. \tag{44}$$

In contrast to the classic zero-mean $\sqrt{M_1}$-ary PAM, the DC bias of such a circularly shifted $\sqrt{M_1}$-ary PAM constellation will result in some extra energy consumption, which therefore results in the above-mentioned SNR loss.

REFERENCES

[1] S.-Y. Li, R. W. Yeung, and N. Cai, "Linear network coding," *IEEE Trans. Inf. Theory.*, vol. 49, no. 2, pp. 371–381, Feb. 2003.
[2] Y. Wu, P. A. Chou, and S.-Y. Kung, "Information exchange in wireless networks with network coding and physical-layer broadcast," Microsoft Research, Redmond, WA, USA, Tech. Rep. MSR-TR-2004, 2004.
[3] Y. Wu, "Broadcasting when receivers know some messages *a priori*," in *Proc. IEEE ISIT*, Nice, France, Jun. 2007, pp. 1141–1145.
[4] L.-L. Xie, "Network coding and random binning for multi-user channels," in *Proc. 10th Can. Workshop Inf. Theory*, 2007, pp. 85–88.

[5] W. Chen, K. B. Letaief, and Z. Cao, "A cross layer method for interference cancellation and network coding in wireless networks," in *Proc. IEEE ICC*, Istanbul, Turkey, Jun. 2006, pp. 3693–3698.
[6] R. Y. Kim and Y. Y. Kim, "Symbol-level random network coded cooperation with hierarchical modulation in relay communication," *IEEE Trans. Consum. Electron.*, vol. 55, no. 3, pp. 1280–1285, Aug. 2009.
[7] J. M. Park, S.-L. Kim, and J. Choi, "Hierarchically modulated network coding for asymmetric two-way relay systems," *IEEE Trans. Veh. Technol.*, vol. 59, no. 5, pp. 2179–2184, Jun. 2010.
[8] W. Chen, Z. Cao, and L. Hanzo, "Maximum Euclidean distance network coded modulation for asymmetric decode-and-forward two-way relaying," *IET Commun.*, vol. 7, no. 10, pp. 2179–2184, Jul. 2013.
[9] W. Chen, L. Hanzo, and Z. Cao, "Network coded modulation for two-way relaying," in *Proc. IEEE WCNC*, Cancun, Mexico, Mar. 2011, pp. 1765–1770.
[10] J. Torrance and L. Hanzo, "Optimisation of switching levels for adaptive modulation in slow Rayleigh fading," *Electron. Lett.*, vol. 32, no. 13, pp. 1167–1169, Jun. 1996.
[11] L. Hanzo, C. H. Wong, and M.-S. Yee, *Adaptive Wireless Transceivers: Turbo-Coded, Turbo-Equalised and Space-Time Coded TDMA, CDMA and OFDM Systems*. Hoboken, NJ, USA: Wiley, 2002.
[12] L. Hanzo, S. X. Ng, W. Webb, and T. Keller, *Quadrature Amplitude Modulation: From Basics to Adaptive Trellis-Coded, Turbo-Equalised and Space-Time Coded OFDM, CDMA and MC-CDMA Systems*. Hoboken, NJ, USA: Wiley, 2004.
[13] S. T. Chung and A. J. Goldsmith, "Degrees of freedom in adaptive modulation: A unified view," *IEEE Trans. Commun.*, vol. 49, no. 9, pp. 1561–1571, Sep. 2001.
[14] A. J. Goldsmith and P. P. Varaiya, "Capacity of fading channels with channel side information," *IEEE Trans. Inf. Theory*, vol. 43, no. 6, pp. 1986–1992, Nov. 1997.
[15] A. J. Goldsmith and S.-G. Chua, "Variable-rate variable-power MQAM for fading channels," *IEEE Trans. Commun.*, vol. 45, no. 10, pp. 1218–1230, Oct. 1997.
[16] B. Choi and L. Hanzo, "Optimum mode-switching-assisted constant-power single-and multicarrier adaptive modulation," *IEEE Trans. Veh. Technol.*, vol. 52, no. 3, pp. 536–560, May 2003.
[17] Q. Liu, S. Zhou, and G. B. Giannakis, "Cross-layer combining of adaptive modulation and coding with truncated ARQ over wireless links," *IEEE Trans. Wireless Commun.*, vol. 3, no. 5, pp. 1746–1755, Sep. 2004.
[18] X. Chen and W. Chen, "Capacity of the broadcasting phase of time-varying two-way relaying," in *Proc. IEEE IWS*, Beijing, China, Apr. 2013, pp. 1–4.
[19] R. O. Afolabi, A. Dadlani, and K. Kim, "Multicast scheduling and resource allocation algorithms for OFDMA-based systems: A survey," *IEEE Commun. Surveys Tuts.*, vol. 15, no. 1, pp. 240–254, 2013.
[20] J. Vella and S. Zammit, "A survey of multicasting over wireless access networks," *IEEE Commun. Surveys Tuts.*, vol. 15, no. 2, pp. 718–753, 2013.
[21] J. Liu, W. Chen, Z. Cao, and K. B. Letaief, "Dynamic power and subcarrier allocation for OFDMA-based wireless multicast systems," in *Proc. IEEE ICC*, Beijing, China, May 2008, pp. 2607–2611.
[22] J. Yuan and K. L. Huang, "Adaptive modulation for MIMO broadcast channels," presented at the *International Conf. Signal Processing Communication Systems*, Gold Coast, Qld, Australia, Dec. 2012, Proc. ICSPCS'07.
[23] A. Goldsmith, *Wireless Communications*. Cambridge, U.K.: Cambridge Univ. Press, 2005.
[24] M. K. Simon and M.-S. Alouini, *Digital Communication Over Fading Channels*. New York, NY, USA: Wiley, 2005.

AQ1 **Yanping Yang** (S'XX) received the B.S. degree in automation and the M.S. degree in electronic engineering from Xidian University, Xi'an China, in 2008, and 2013, respectively. He is currently studying in the Department of Electronic Engineering, Tsinghua University, Beijing, China. He is pursuing the Ph.D. degree in National Digital Switching System Engineering and Technological R&D Center, Zhengzhou, China.

His research interests include wireless communications and cognitive radio networks. He currently serves as a Reviewer for the IEEE Wireless Communications Letters, the IEEE ICCS, and the IEEE ATC.

Wei Chen (S'05–M'07–SM'13) received the B.S. and Ph.D. degrees in electronic engineering (both with the highest honors) from Tsinghua University, Beijing, China, in 2002, and 2007, respectively. From 2005 to 2007, he was also a visiting research staff member in the Hong Kong University of Science and Technology (HKUST). Since July 2007, he has been with Department of Electronic Engineering, Tsinghua University, where he is a Full Professor and the Chair of department teaching committee. He visited the University of Southampton, UK, from June 2010 to Sept. 2010, and Telecom ParisTech, France, from June 2014 to Sept. 2014. Dr. Chen is a 973 Youth Project chief scientist and a national young and middle-aged leader for science and technology innovation. He is also supported by the NSFC excellent young investigator project, new century talent program of Ministry of Education, Beijing nova program, and 100 fundamental research talents program of Tsinghua University (also known as 221 talents Program).

His research interests are in areas of wireless communications, information theory, and applied optimizations. He serves as Editor for IEEE TRANSACTIONS ON EDUCATION, IEEE WIRELESS COMMUNICATIONS LETTERS, and China Communications, as a Vice Director of youth committee of China Institute of Communications. He served as a tutorial co-chair of the 2013 IEEE ICC, a TPC co-chair of 2011 Spring IEEE VTC, and symposium co-chairs for IEEE ICC, ICCC, and CCNC. He was the recipient of the First Prize of 14th Henry Fok Ying-Tung Young Faculty Award, the 2010 IEEE Comsoc Asia Pacific Board Best Young Researcher Award, the 2009 IEEE Marconi Prize Paper Award, the Best Paper Awards at IEEE ICC 2006, IEEE IWCLD 2007, and IEEE Smart Gird Com. 2012, the 2011 Tsinghua Raising Academic Star Award. Prof. Chen holds the honorary titles of Beijing excellent teacher and Beijing excellent young talent. He is the Champion of the first national young faculty teaching competition, and a winner of National May 1st Medal.

Ou Li received the Ph.D. degree from National Digital Switching System Engineering and Technological Research Center (NDSC), Zhengzhou, China, in 2001. He is currently a Professor at NDSC in China.

His primary research interests include wireless communication technology, wireless sensor network and cognitive radio networks.

Lajos Hanzo (F'XX) received the degree in electronics in 1976 and his doctorate in 1983. In 2009 he was awarded the honorary doctorate "Doctor Honoris Causa" by the Technical University of Budapest. During his 38-year career in telecommunications he has held various research and academic posts in Hungary, Germany and the UK. Since 1986 he has been with the School of Electronics and Computer Science, University of Southampton, UK, where he holds the chair in telecommunications. He has successfully supervised about 100 PhD students, co-authored 20 John Wiley/IEEE Press books on mobile radio communications totalling in excess of 10 000 pages, published 1400+research entries at IEEE Xplore, acted both as TPC and General Chair of IEEE conferences, presented keynote lectures and has been awarded a number of distinctions. Currently he is directing a 100-strong academic research team, working on a range of research projects in the field of wireless multimedia communications sponsored by industry, the Engineering and Physical Sciences Research Council (EPSRC) UK, the European Research Council's Advanced Fellow Grant and the Royal Society's Wolfson Research Merit Award. He is an enthusiastic supporter of industrial and academic liaison and he offers a range of industrial courses. He is also a Governor of the IEEE VTS. During 2008–2012 he was the Editor-in-Chief of the IEEE Press and a Chaired Professor also at Tsinghua University, Beijing. His research is funded by the European Research Council's Senior Research Fellow Grant. For further information on research in progress and associated publications please refer to http://www-mobile.ecs.soton.ac.uk Lajos has 20 000+citations. AQ2

AUTHOR QUERIES

AUTHOR PLEASE ANSWER ALL QUERIES

AQ1 = Please provide field of membership year.
AQ2 = Please provide field of membership year.

END OF ALL QUERIES

Variable-Rate, Variable-Power Network-Coded-QAM/PSK for Bi-Directional Relaying Over Fading Channels

Yanping Yang, *Student Member, IEEE*, Wei Chen, *Senior Member, IEEE*, Ou Li, and Lajos Hanzo, *Fellow, IEEE*

***Abstract*—Network coded modulation (NCM) holds the promise of significantly improving the efficiency of two-way wireless relaying. In this contribution, we propose near instantaneously adaptive variable-rate, variable-power QAM/PSK for NC-aided decode-and-forward two-way relaying (DF-TWR) to maximize the average throughput. The proposed scheme is optimized subject to both average-power and bit-error-ratio (BER) constraints. Based on the BER bounds, we investigate a discrete-rate adaptation scheme, relying on a pair of solutions proposed for maximizing the spectral efficiency of the network. We then derive a closed-form solution based power adaptation policy for a continuous-rate scheme and quantify the signal-to-noise ratio (SNR) loss imposed by NC-QAM. Our simulation results demonstrate that the proposed discrete adaptive NC-QAM/PSK schemes are capable of attaining a higher spectral efficiency than their fixed-power counterparts.**

***Index Terms*—Network coded modulation, adaptive modulation, two-way relaying, fading channels, spectral efficiency.**

I. Introduction

Two-way relaying (TWR), also known as bi-directional relaying, constitutes an appealing technique of improving the throughput of the existing wireless network. The landmark contribution of Li, Yeung and Cai [1] put forward the linear Network Coding (NC) concept for single-source multicast networks for the sake of approaching the max-flow bound of the information transmission rate. Inspired by this work, a variety of NC methods have been proposed [2]–[9]. To the best of our knowledge, [2] was the first contribution that combined NC with the physical layer broadcast capability of the wireless medium, which is capable of improving the achievable throughput with the aid of the modulo-two based superposition of sequences. From an information theoretic view, Wu [3] and Xie [4] investigated the downlink (DL) capacity of asymmetric Decoded-and-Forward Two-Way Relaying (DF-TWR). More practically, NC was jointly designed with superposition coding in [5], where the authors proposed a cross-layer method for joint interference cancellation and network coding in multi-hop wireless networks, which may substantially improve the capacity regions, whilst reducing the power dissipated at the relay node. Symbol level NC was investigated in [6], which is capable of improving the asymmetric[1] relay throughput using hierarchical modulation. The joint design of NC and modulation was investigated in [7], which alleviated the asymmetric relaying-induced problems in TWR networks. Based on a set-partitioning algorithm, both NC-QAM/PSK and a NC oriented maximum ratio combining (MRC) technique was conceived for improving both the throughput as well as the achievable spatial diversity gain at a low complexity [8], [9], which circumvented the asymmetric transmission problems of DF-TWR. For the sake of maximizing the data rates of two-way links under certain BER constraints, constant-power, variable-rate adaptive Network-Coded Modulation (NCM) was proposed in [8]. This motivates our research on how to design variable-power, variable-rate adaptive NCM for TWR, because it is beneficial to consider joint power and rate allocation schemes for time-varying fading channels.

Inspired by the above-mentioned solutions, improving the spectral efficiency for transmission over fading channels has gradually become the focus of the related research [10]–[17]. As one of the key techniques that has found its way into both current and future wireless systems, adaptive modulation has received extensive attentions. Hanzo *et al.* designed diverse near-instantaneously adaptive modulation techniques in [10]–[12]. Based on Shannon capacity and BER bounds, Goldsmith *et al.* [13]–[15] investigated point-to-point adaptive modulation schemes for flat-fading channels, where both the data rate and the transmit power were near-instantaneously adapted for the sake of maximizing the spectral efficiency, whilst maintaining a constant BER. In [16], constant-power single- and multicarrier adaptive quadrature amplitude modulation (AQAM) was

Manuscript received March 28, 2014; revised July 22, 2014; accepted August 26, 2014. This paper was supported in part by the National Basic Research Program of China (973 Program) under Grant 2013CB336600, by NSFC Excellent Young Investigator Award 61322111, by NSFC Project 61201380, by the National High Technology Research and Development Program of China (863 Program) under Grant 2012AA121606, by the National Innovative Talents Promotion Program 2013RA2151, by the MoE New Century Talent Program NCET-12-0302, by Beijing Nova Program Z121101002512051, and by the National Science and Technology Key Project 2013ZX03003006-005. The associate editor coordinating the review of this paper and approving it for publication was J. Yuan.

Y. Yang is with the National Digital Switching System Engineering and Technological R&D Center, Zhengzhou 450002, China. He is also with the Department of Electronic Engineering, Tsinghua University, Beijing 100084, China (e-mail: y.p.yang1986@gmail.com).

W. Chen is with the Department of Electronic Engineering, Tsinghua University, Beijing 100084, China (e-mail: wchen@tsinghua.edu.cn).

O. Li is with the National Digital Switching System Engineering & Technological R&D Center, Zhengzhou 450002, China (e-mail: zzliou@126.com).

L. Hanzo is with the School of Electronics and Computer Science, University of Southampton, Southampton SO17 1BJ, U.K. (e-mail: lh@ecs.soton.ac.uk).

Digital Object Identifier 10.1109/TCOMM.2014.2354353

[1]The asymmetry here implies that the two-way traffic flows may have different symbol rates.

investigated compared to variable-power variable-rate M-ary QAM (MQAM) proposed in [15]. Following the similar approach of [15], Liu *et al.* developed a cross-layer design in [17], which combines adaptive modulation and coding at the physical layer combined with a truncated Automatic Repeat reQuest (ARQ) protocol at the data link layer. These adaptive modulation contributions studied single-user transmission, relying on a single channel's quality. This motivates us to intrinsically amalgamate adaptive modulation with TWR where the downlink streaming from the relay (R) to both destinations (D) has to simultaneously adapt to a pair of channel conditions.

Since the R-D DL of TWR is equivalent to the classic broadcast channel (BC) relying on side information, we consult the relevant literature on adaptive modulation conceived for both broadcast channels and for multicast systems [18]–[22]. Specifically, the authors of [18] investigated both the achievable channel capacity and the power allocation of the downlink of time-varying TWR. The resource allocation of multicast systems was discussed in [19]–[21], while the adaptive modulation aided multiple-input, multiple-output (MIMO) downlink channel was studied in [22]. To the best of our knowledge, there is a paucity of contributions on the joint power and rate allocation of near-instantaneously adaptive NCM schemes designed for broadcast channels or multicast systems. This is because the BC channel has to dispense with power adaptation at the transmitter without the knowledge of the users' channel state information (CSI). However, gleaming perfect CSI for a large user-population is unrealistic in broadcast channels or multicast systems. Therefore, the transmitter usually transmits its messages at a fixed power and using fixed modulation modes, rather than implementing power adaptation. However, in the downlink of TWR, there are only two users. Therefore the two user's accurate CSI can be relatively easily obtained at the relay node. Hence we embark on investigating the two users' joint power and rate allocation problem in the context of TWR by relying on perfect CSI.

Therefore we take the challenge of designing joint power and rate adaptation aided NCM for the DF-TWR DL relying on side information. Compared to the conventional single-user adaptive modulation scheme of [15], the main differences can be summarized as follows:

i) Instead of a single channel, the power allocation strategy of our proposed scheme has to simultaneously adapt to a pair of channel conditions;
ii) The pair of R-D links are coupled due to the SNR loss imposed by NC-QAM, which implies that the user who has a lower transmit rate will suffer from an SNR loss [8];
iii) When we investigate a discrete-rate adaptive scheme, a specific transmit power results in two different transmit rates, depending on the two links' CSI. However, the power and the two rates cannot be optimally matched. Explicitly, when one user achieves its optimal power and rate match, it is highly likely that for the other user, the power will be higher than the user's modulation mode actually needs at this moment, which implies that there is a power-loss. Alternatively at a given power this may be viewed as a rate-loss. By contrast, in [15], the power and rate allocation is always optimal. In conclusion, the combination of joint power and rate adaptive modulation aided NCM requires more sophisticated design than that of conventional single-user adaptive modulation.

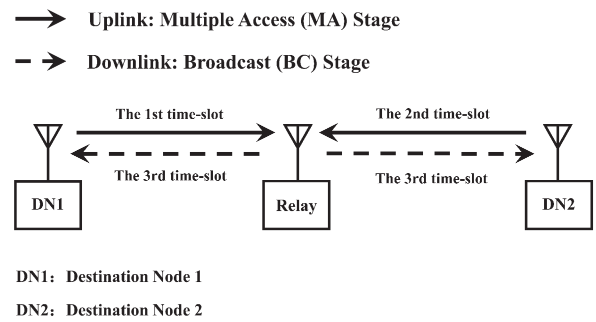

Fig. 1. System model of DF-TWR (Three-timeslot TWR).

Based on the idea of intrinsically amalgamating NCM and adaptive modulation, we propose near-instantaneously adaptive NC-QAM/PSK for the downlink of DF-TWR, which can be regarded as a joint optimization with the objective of maximizing the capacity of networks. As the RN simultaneously broadcasts its signals to two receiver nodes, the same transmit power has to adapt to both fading channel conditions. Therefore the key challenge for the scheme is to optimize both the transmit power and the transmit rates for the sake of maximizing the achievable spectral efficiency, while satisfying the average power and BER constraints. To solve this optimization problem, firstly, we proposed a solution for a discrete-rate scheme based on the so-called fading region partitioning method. Secondly, a closed-form solution is derived for the power adaptation policy of a continuous-rate adaptive scheme. Finally, on the basis of this continuous-rate solution, we conceive another discrete-rate scheme by invoking a continuous-rate discretization method. Based on the above arguments it may be concluded that the most significant contribution of this paper is the joint adaptive allocation of power and rate for NCM. The proposed adaptive NC-QAM/PSK scheme conceived for DF-TWR is capable of beneficially improving the achievable spectral efficiency, therefore holds the promise of rich near-future applications.

The rest of this paper is organised as follows. Section II presents our system model, while Section III describes our unified adaptive NCM optimization problem, followed by a pair of discrete-rate solutions proposed for practical scenarios which are applicable to arbitrary constellations. Section IV presents our simulation results for characterizing our adaptive NC-QAM/PSK, while our concluding remarks are provided in Section V.

II. System Model

Consider the DF-TWR network associated with a multicarrier system, which employs time division duplexing. Fig. 1 shows an abridged general view of a three-timeslot bidirectional transmission system, which includes two destination nodes and a relay node. Destination node 1 (DN1) and DN2 in the DL also act as source nodes (SN) during the uplink transmission stage. The information exchange between the two DNs can be divided into two distinct stages: the multiple access (MA) stage when the two nodes separately send their data to the

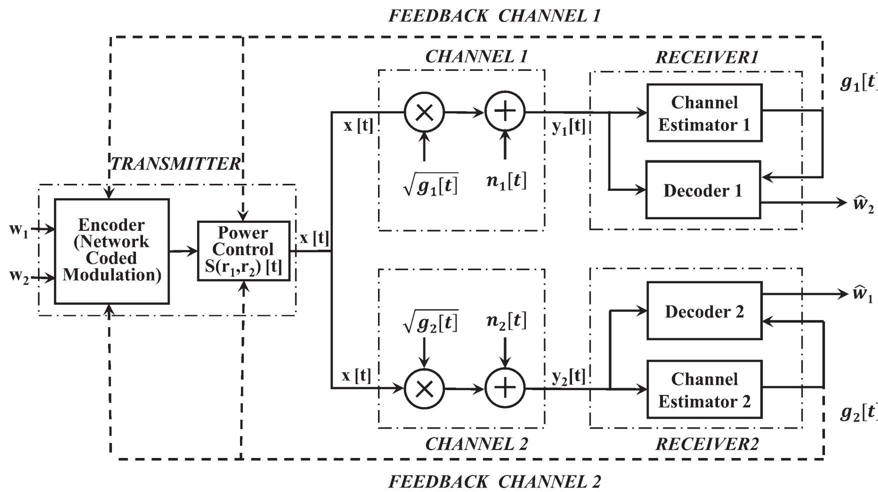

Fig. 2. System model of adaptive NC-QAM/PSK for DF-TWR.

relay, and the broadcast (BC) stage, when the relay broadcasts the combined signal to both DN1 and DN2. Each DN has *a priori* knowledge of its own message intended for the other.

Based on the above-mentioned TWR model, we then construct the adaptive NC-QAM/PSK system model of Fig. 2, where the key part of the scheme is the transmitter design, constituted by the NCM design and the adaptive modulation design. Since the fixed-mode NCM has already been richly studied in [8], we focus our attention on adaptive NCM conceived for near-instantaneously time-varying fading channels. Accordingly, we describe the system model of adaptive NC-QAM/PSK.

Before introducing the system's structure, we first list the assumptions adopted in this paper:

A1) The channel is a non-dispersive and slowly-varying Rayleigh fading channel. When the channel is changing faster than it can be estimated and fed back to the transmitter, adaptive techniques will perform poorly.

A2) Perfect channel state information (CSI) is available both at the relay as well as at DN1 and DN2 using training-based channel estimation. The idealized simplifying assumption that the feedback path does not introduce any errors and has no latency may be approximately satisfied by using a low-delay feedback link relying on powerful error control. The practical system design relying on delayed or noisy CSI [15] is left for our future investigations.

A3) Linear modulation is used, where the adaptation takes place at integer multiples of the symbol rate of $R_s = 1/T_s$, where T_s denotes the symbol duration. It is also assumed that the system uses ideal Nyquist criterion, having a bandwidth of $B = 1/T_s$. We assume having a non-dispersive discrete-time downlink channel having stationary ergodic time-varying gains of $\sqrt{g_i[t]}, i = 1, 2$ contaminated by the additive white Gaussian noise (AWGN) $n_i[t]$, where t denotes the time instants.

We conceive the NCM design according to [8]. In this paper, we only focus our attention on the DL of DF-TWR, where the messages at the RN are processed and broadcast to DN1 and DN2 using NC-QAM/PSK. In the static asymmetric DF-TWR DL, the equivalent baseband signals received at the coherent receiver of DN1 and DN2 are represented by

$$Y_i = h_i X + Z_i, i = 1, 2, \tag{1}$$

where the channel gains are denoted by $|h_i|^2 = g_i$, with g_i representing the power gains. The transmit symbol at the RN is denoted by X, while Z_i represent the AWGN at DN1 and DN2.

Without loss of generality, we assume that the transmit constellation sizes are denoted by M_1, M_2, let $M_2 \geq M_1$, $M_2/M_1 = \mathbb{N}$. The messages w_1, w_2 to be transmitted from the pair of source nodes will be merged into a single signal (denoted by X) using the modulo-two operation at the relay [8]. For QAM, the messages w_1, w_2 then will be respectively mapped to symbols from the set of M-ary QAM constellation points, which is formulated as

$$\chi_i = \left\{2\sqrt{M_i}\left(a_i^I + ja_i^Q\right) - \left(\sqrt{M_i} - 1\right)(1+j) : a_i^I, a_i^Q \in \mathcal{A}_i\right\}, \tag{2}$$

where

$$\mathcal{A}_i = \begin{cases} \left\{0, \frac{1}{2}\right\}, & \text{if } M_i = 4 \\ \left\{0, \frac{1}{\sqrt{M_i}}, \frac{2}{\sqrt{M_i}}, \ldots, \frac{\sqrt{M_i}-1}{\sqrt{M_i}}\right\}, & \text{if } M_i > 4 \end{cases}, \quad i = 1, 2 \tag{3}$$

where $M_i \in \{4, 16, 64, \ldots\}$ for QAM. Given the normalised amplitudes (a_1^I, a_1^Q) and (a_2^I, a_2^Q), the transmitter will generate the NC-QAM symbol as

$$X = d\left[2\sqrt{M_2}(a^I + ja^Q) - \left(\sqrt{M_2} - 1\right)(1+j)\right], \tag{4}$$

where we have $d = \sqrt{((3E_s)/2(M_2 - 1) - 1))}$, $M_2 > M_1$, while d denotes half of the symbol-distance in QAM, given an energy of E_s per symbol. The normalised amplitudes are given by

$$\begin{cases} a^I = a_1^I + a_2^I, \bmod 1 \\ a^Q = a_1^Q + a_2^Q, \bmod 1. \end{cases} \tag{5}$$

For NC-PSK, w_1, w_2 will be mapped to the symbols χ_1, χ_2 chosen from a normalised M-ary PSK (MPSK) constellation, as in $\chi_i = \{\cos\theta_i + j\sin\theta_i : \theta_i \in \Theta_i\}$, where we have

$$\Theta_i = \left\{0, \frac{2\pi}{M_i}, \ldots, \frac{2(M_i - 1)\pi}{M_i}\right\}, \quad i = 1, 2, \tag{6}$$

where $M_i \in \{2, 4, 8, 16, \ldots\}$ for PSK. Given the phases θ_1 and θ_2, the transmitter generates an NC-PSK symbol given by

$$X = \sqrt{E_s}\left(\cos\theta + j\sin\theta\right), \tag{7}$$

where E_s denotes the symbol energy, while the symbol's phase θ is given by

$$\theta = \theta_1 + \theta_2 \mod 2\pi. \tag{8}$$

We then conceive near-instantaneously adaptive NCM for time-varying fading channels where the modulated signals will be represented by the signal sequence in the system model of Fig. 2. Therefore the previous symbol X will be represented as $x[t]$, while Y will be represented by $y_i[t], i = 1, 2$.

Let us now describe our adaptive transmission scheme seen in Fig. 2. We consider discrete-time (t denotes discrete time instants) flat fading channels adhering to the assumptions A1)–A3), where the transmitter (relay) dynamically adjust both its transmit power and transmit rates according to the power gains $g_1[t]$ and $g_2[t]$ signalled to it from the two receivers (DN1 and DN2). Let us denote the average transmit power by $\overline{S}$, the noise density of $n_i[t]$ by $(N_0/2)$, the channel gain by $g_i[t]$ and the average channel gain by $\overline{g}$. For a constant transmit power $\overline{S}$, the instantaneous received SNRs are $\gamma_i[t] = \overline{S}g_i[t]/(N_{0_i}B)$. Upon normalization by $\overline{S}$, we can assume that $\overline{g} = 1$. Then the average received SNRs are $\overline{\gamma}_i = \overline{S}/(N_{0_i}B)$. We denote the probability distribution of the received SNR by $p(\gamma_i) = p(\gamma_i[t] = \gamma_i)$. In this paper, the fading distributions $p(\gamma_i)$ are assumed to be either lognormal or exponential (Rayleigh fading). When the context is unambiguous, we will omit the time reference t related to n_i, g_i, γ_i and $\overline{\gamma}_i$.

The above-mentioned two designs constitute the fundamental framework of our adaptive NC-QAM/PSK scheme. Specifically, the assumption of A2) signifies that the feedback channel is error free and has no latency, which could be at least approximately satisfied by using a fast feedback link with powerful error control for feedback information. The feedback path delays are not shown in Fig. 2.

III. Adaptive Network Coded M-ary Modulation

In Section II we discussed the general system model of adaptive NC-QAM/PSK. In this section we will describe the specific form of adaptive NC-QAM/PSK aided DF-TWR, where both the rate and the transmit power of M-ary QAM/PSK are varied near-instantaneously for the sake of maximizing the spectral efficiency, while meeting the BER targets. We study this specific form of adaptive NCM in the context of the downlink of DF-TWR. Therefore, the main emphasis of this paper is on practical adaptive modulation and on its spectral efficiency normalized to the theoretical maximum. The remainder of this section is organized as follows. In Subsection A, we describe the optimization problem of our variable-rate, variable-power NC-QAM/PSK scheme. The spectral efficiency of our discrete-rate, continuous-power scheme is discussed in Subsection B. We then investigate the continuous-rate, continuous-power adaptive scheme in Subsection C. Finally, we propose a continuous-rate discretization method in Subsection D. Before analyzing our adaptive schemes, we would like to first list some of the notations used.

- $M_i(\gamma_i)$: denotes the constellation sizes that are used in the continuous-rate scheme (Section III-C), with their domains being $M_i(\gamma_i) \geq 1$.
- $M_{1,\eta}$, $M_{2,\delta}$: denotes the constellation sizes that are used in discrete-rate schemes (Section III-B and D), which implies that receiver 1 (or 2) adopt the transmission modes η (or δ). Usually their values are discrete and are larger than 2.
- $k(\gamma_i)$: denotes the continuous transmit rates.
- $k_{1,\eta}$, $k_{2,\delta}$: denotes the discrete transmit rates.
- λ_i. denotes the SNR-loss imposed by NC-QAM. We included the derivation of SNR-loss in the Appendix.
- $S(\gamma_1, \gamma_2)$: denotes the continuous instantaneous transmit power, which is related to instantaneous SNR γ_1 and γ_2.
- $S_{\eta\delta}(\gamma_1, \gamma_2)$: denotes the discrete instantaneous transmit power, which corresponds to the transmission modes η and δ.
- ω_i: denotes the weighting coefficients of the relay-DN1 link and relay-DN2 link, respectively.

A. *Unified Problem Formulation for Adaptive NC-QAM/PSK*

Again, the emphasis of this contribution is on the transmitter design relying on the CSI knowledge, therefore it is necessary to derive the basic formulas required for the transmitter's design. Based on these formulas we unify the basic optimization problem for adaptive NC-QAM/PSK, which will be discussed in Subsections B, C and D.

1) The Achievable Rate for the Downlink of the TWR: According to Section II, when the time reference t can be omitted, without any ambiguity we may rewrite the expression of the corresponding parameters as $\gamma_i, i = 1, 2$, $\overline{\gamma}_i$ and $p(\gamma_i)$, which will be used in deriving the system's capacity. The capacity of fading channels for DF-TWR is limited by both the transmit power and bandwidth available. Let $S(\gamma_1, \gamma_2)$ denote the transmit power relative to the instantaneous SNR γ_1 and γ_2, subject to the average power constraint of

$$\int_0^\infty \int_0^\infty S(\gamma_1, \gamma_2) p(\gamma_1) p(\gamma_2) d\gamma_1 d\gamma_2 = \bar{S}, \tag{9}$$

where $p(\gamma_1)$ is independent of $p(\gamma_2)$. When considering a Rayleigh fading channel for example, we have

$$p(\gamma_i) = \frac{1}{\overline{\gamma_i}} e^{-\gamma_i/\overline{\gamma_i}}, \quad i = 1, 2, \tag{10}$$

where $\overline{\gamma_i} = \overline{S}T_s/N_0 = \overline{E_s}/N_0$ denotes the average SNR per symbol, $T_s = 1/B$.

The BER performance of NC-QAM/PSK matches well with the theoretical BER expressions provided in [8], [23]. However, the theoretical BER expressions contain the Q-function [24], which is hard to invert. In our proposed adaptive NC-QAM/PSK scheme, we use Error Probability Bounds (EPBs) ([23, Chapter 9]) instead of the theoretical BER expressions ([23, Table 6.1]). Particularly, NC-QAM exhibits a modest SNR loss, when the selected constellation sizes of the DN1 and DN2 are different [8]. Therefore the concept of the SNR-loss coefficients λ_1, λ_2 will be introduced into our BER expressions. However, there is no SNR-loss for NC-PSK [8]. To unify these expressions, we introduce the same coefficients, but let $\lambda_1 = \lambda_2 = 1$ for NC-PSK.

The unified approximation BER bound has been provided in [23, Chapter 9.4]. If we consider the above-mentioned SNR-loss and write the BER bound [23] in a pairwise form, then we arrive at:

$$\begin{cases} P_{b_1}(\gamma_1) \le c_1 \exp\left[\frac{-c_2\lambda_1\gamma_1\frac{S(\gamma_1,\gamma_2)}{\bar{S}}}{2^{c_3k(\gamma_1)}-c_4}\right] \\ P_{b_2}(\gamma_2) \le c_1 \exp\left[\frac{-c_2\lambda_2\gamma_2\frac{S(\gamma_1,\gamma_2)}{\bar{S}}}{2^{c_3k(\gamma_2)}-c_4}\right], \end{cases} \tag{11}$$

where c_1, c_2 and c_3 are fixed positive constants, while c_4 is a real constant. The received SNRs now become $\gamma_i S(\gamma_1, \gamma_2)/\bar{S}$, $i = 1, 2$. The transmit rates $k(\gamma_1)$, $k(\gamma_2)$ hence become

$$k(\gamma_i) = \frac{\log_2 M_i(\gamma_i)}{c_3}, \quad i = 1, 2, \tag{12}$$

where $M_i(\gamma_i)$ represents the constellation sizes, while the SNR-loss coefficients λ_1 and λ_2 are

$$\lambda_i = \begin{cases} \frac{1-M_i^{-1}(\gamma_i)}{1-M_1^{-1}(\gamma_1)}, \text{if } M_1(\gamma_1) \ge M_2(\gamma_2) \ge 1, i = 1,2 \\ \frac{1-M_i^{-1}(\gamma_i)}{1-M_2^{-1}(\gamma_2)}, \text{if } M_2(\gamma_2) \ge M_1(\gamma_1) \ge 1, i = 1,2 \\ 1,\ NC-PSK scheme. \end{cases} \tag{13}$$

The SNR-loss coefficients are obtained according to Paragraph 1, Line 10 of the Appendix, where for the sake of streamlining the related formula, we let $\lambda_1 = \lambda_2 = 1$ for NC-PSK. Of particular note is that in Eq. (13), the values of the constellation sizes $M_1(\gamma_1)$ and $M_2(\gamma_2)$ are continuous, with their domains being $[1, \infty)$.

From Eq. (13) we see that when the MQAM constellation sizes $M_1(\gamma_1)$ and $M_2(\gamma_2)$ are fixed and different, an SNR loss is imposed at the destination node having a lower-order constellation size. Fortunately, the SNR loss decreases upon increasing the receiver-side SNR, which means that higher-order modulations can be used. We will carry out the related analysis according to the different scenarios in the subsequent subsections.

Throughout this paper, the BER bounds of MQAM are given by ([23, Eqs. (9.6) and (9.7)]), where we have $c_1 = 2$ or 0.2, $c_2 = 1.5$, $c_3 = 1$ and $c_4 = 1$. The SNR-loss coefficients $\lambda_i, i = 1, 2$ are given by Eq. (13). By contrast, the BER bound of MPSK is given by ([23, Eq. (9.49)]), with $c_1 = 0.05$, $c_2 = 6$, $c_3 = 1.9$, $c_4 = 1$. Specifically, we have $\lambda_i = 1, i = 1, 2$ for MPSK.

To facilitate our forthcoming discussions and calculations, Eq. (11) may be reformulated as

$$M_i(\gamma_i) \le c_4 + K_i\lambda_i\gamma_i\frac{S(\gamma_1,\gamma_2)}{\bar{S}},\ i = 1, 2, \tag{14}$$

where

$$K_i = -\frac{c_2}{\ln\left(P_{b_i}/c_1\right)}. \tag{15}$$

These BER bounds may be expected to closely approximate the accurate BER expressions and may also be readily inverted. Therefore we can obtain $M_i(\gamma_i)$ or $k(\gamma_i)$ as a function of P_{b_i} and $S(\gamma_1, \gamma_2)$.

2) Variable-Rate, Variable-Power NC-QAM/PSK: Let us now discuss the capacity of variable-rate, variable-power NC-QAM/PSK for the downlink of DF-TWR. As seen in Fig. 2, in a fading channel where the relay broadcasts its signals to both DN1 and DN2, the receiver side SNR γ_1, γ_2 fluctuates as a function of time. We adjust $S(\gamma_1, \gamma_2)$ according to γ_1, γ_2, under the average power constraint of $\bar{S}$.

Our optimization problem is then formulated as that of maximizing the spectral efficiency of adaptive NCM. Let $R[\gamma_1, \gamma_2, S(\gamma_1, \gamma_2)]$ denote the available rate as a function of γ_1, γ_2 and $S(\gamma_1, \gamma_2)$, which is expressed as

$$R\left[\gamma_1, \gamma_2, S(\gamma_1, \gamma_2)\right] = \sum_{i=1}^{2}\frac{\omega_i}{c_3}\log_2 M_i(\gamma_i), \quad i = 1, 2, \tag{16}$$

where $M_i(\gamma_i)$ is given by Eq. (14), ω_1 denotes the significance of the DN1 channel, while that of the DN2 channel is ω_2. Naturally, we have $\omega_1 + \omega_2 = 1$ and $0 \le \omega_i \le 1, i = 1, 2$.

The achievable spectral efficiency is obtained by integrating the rate function over the fading region D. We then unify the optimization problem as follows:

$$\begin{aligned} &\text{maximize } \frac{R}{B} = \iint_D R[\gamma_1,\gamma_2, S(\gamma_1,\gamma_2)]p(\gamma_1)p(\gamma_2)d\gamma_1 d\gamma_2 \\ &\text{subject to } \quad \iint_D S(\gamma_1,\gamma_2)p(\gamma_1)p(\gamma_2)d\gamma_1 d\gamma_2 = \bar{S} \\ &\qquad\qquad\quad S(\gamma_1,\gamma_2) \ge 0 \\ &\qquad\qquad\quad D = \mathbb{R}^2, \end{aligned} \tag{17}$$

where $\bar{S}$, $S(\gamma_1, \gamma_2)$, γ_i, B, $p(\gamma_i)$ were defined as that of our system model.

Since the logarithmic functions in Eq. (16) are concave and so is their sum, Eq. (17) constitutes a convex optimization problem. We form the Lagrangian by exploiting the Karush–Kuhn–Tucker (KKT) condition similarly to the approach of [18], where υ^* and μ^* are Lagrange multipliers. In particular, for the discrete-rate scheme, the integration area D is divided into sub-areas denoted by $D_{\eta,\delta}$, which are used as our optimization variables.

We are now in the position to conceive two different adaptive schemes, namely a discrete-rate, continuous-power NC-QAM/PSK and a continuous-rate, continuous-power NC-QAM/PSK arrangement. For the former optimization problem, not only the transmit power adaptation policy, but also the fading region division requires further discussions. For the latter scheme, we just have to find the optimal power adaptation policy that maximizes the achievable spectral efficiency, which is formulated as Eq. (18), shown at the bottom of the next page.

Eq. (17) presents a general formulation of the adaptive NC-QAM/PSK optimization problem. In the following subsections, both the discrete-rate, continuous-power and the continuous-rate, continuous-power adaptive schemes will be investigated in detail.

B. Discrete-Rate Adaptive M-ary QAM/PSK

According to the optimization problem formulated in the previous subsection, we conceive a practical solution for adaptive NC-QAM/PSK, which is referred to as our discrete-rate, continuous-power DF-TWR scheme. Explicitly, in the traditional single-user continuous-rate adaptation scheme we have to find the optimal cutoff fade depth parameter υ^*[15], whilst in the proposed discrete-rate schemes, our goal is that of finding the joint optimal power and rate for the pair of independent fading distributions of the relay-DN1 and relay-DN2 links. This issue will be discussed first, followed by a solution for our discrete variable-rate, variable-power NC-QAM/PSK scheme.

Similarly to our previous system model, the BER bounds of Eq. (11) and its rearranged form in Eq. (14) constitute the basis of our discussions. In the joint-optimization scheme destined for the receivers DN1 and DN2, the transmit rates are denoted by $k_{1,\eta}$ and $k_{2,\delta}$, which directly depend on the constellation sizes $M_{1,\eta}$ and $M_{2,\delta}$ as follows:

$$\begin{cases} k_{1,\eta} = \frac{\log_2 M_{1,\eta}}{c_3} \\ k_{2,\delta} = \frac{\log_2 M_{2,\delta}}{c_3}. \end{cases} \tag{19}$$

For each receiver side at DN1 and DN2, we adopt the single-user partitioning method of [15]. Specifically, we consider the discrete sets of MQAM/MPSK transmission modes $\mathcal{M}_1 = \{M_{1,0}, \ldots, M_{1,N_1-1}\}$, $\mathcal{M}_2 = \{M_{2,0}, \ldots, M_{2,N_2-1}\}$, with $M_{1,0}=0$ and $M_{2,0}=0$ implying no transmission. The receiver-side SNR distributions are then divided into N_1 and N_2 fading-magnitude regions denoted by $R_{1,n_1} = [\gamma_{1,n_1-1}, \gamma_{1,n_1}), n_1 = 0, \ldots, N_1-1$, $R_{2,n_2} = [\gamma_{2,n_2-1}, \gamma_{2,n_2}), n_2 = 0, \ldots, N_2-1$, where $\gamma_{i,-1}=0, \gamma_{i,N_i-1}=\infty, i=1,2$. We then activate the pair of fixed constellation sizes of M_{1,n_1}, M_{2,n_2}, when the receiver side SNRs obey $\gamma_1 \in R_{1,n_1}$, $\gamma_2 \in R_{2,n_2}$.

According to the above fading-magnitude partitioning method and to the basic optimization problem of Eq. (17), we have now formulated our basic discrete-rate scheme for DF-TWR. The associated power control policy conceived for joint-optimization should now be discussed further. Let $S_{\eta\delta}(\gamma_1,\gamma_2), \eta \in \{0,1,\ldots, N_1-1\}$, $\delta \in \{0,1,\ldots,N_2-1\}$ denote the relay's transmit power for $\gamma_1 \in R_{1,n_1}$, $\gamma_2 \in R_{2,n_2}$. From Eq. (14) we arrive at:

$$\begin{cases} \frac{S_{\eta\delta}(\gamma_1,\gamma_2)}{\bar{S}} \geq \frac{M_{1,\eta}-c_4}{\lambda_1 K_1 \gamma_1} \\ \frac{S_{\eta\delta}(\gamma_1,\gamma_2)}{\bar{S}} \geq \frac{M_{2,\delta}-c_4}{\lambda_2 K_2 \gamma_2}, \end{cases} \tag{20}$$

where γ_1, γ_2, c_4, K_1, K_2, λ_1, and λ_2 are derived as part of previous subsection. For MQAM, λ_1, λ_2 are given by Eq. (13), whereas for MPSK, we have $\lambda_1 = \lambda_2 = 1$.

The most important difference between our discrete-rate and continuous-rate schemes is that in the discrete-rate scheme, the inequalities in Eq. (20) cannot assume equality at the same time. Since the rates only have discrete values, therefore a fixed $S_{\eta\delta}(\gamma_1,\gamma_2)$ cannot satisfy both equations simultaneously, except when $\gamma_1 = \gamma_2$, which is practically impossible in time-varying fading channels. Similarly to the single-user variable-rate, variable-power MQAM scheme discussed in [15], our proposed discrete-rate scheme cannot achieve the optimal performance of the continuous-rate adaptive scheme to be studied in Subsection C, hence there is an inevitable power-loss or rate-loss. Let us now continue by making some reasonable adjustments to our power control policy. Let

$$\frac{S_{\eta\delta}(\gamma_1,\gamma_2)}{\bar{S}} = \max\left\{\frac{M_{1,\eta}-c_4}{\lambda_1 K_1 \gamma_1}, \frac{M_{2,\delta}-c_4}{\lambda_2 K_2 \gamma_2}, 0\right\}, \tag{21}$$

where we have

$$\begin{cases} \lambda_1 = 1, \lambda_2 = \frac{1-M_{2,\delta}^{-1}}{1-M_{1,\eta}^{-1}},\ if\ M_{1,\eta} \geq M_{2,\delta} \geq 2 \\ \lambda_1 = \frac{1-M_{1,\eta}^{-1}}{1-M_{2,\delta}^{-1}}, \lambda_2 = 1,\ if\ M_{2,\delta} \geq M_{1,\eta} \geq 2 \\ \lambda_1 = 1, \lambda_2 = 1,\ NC-PSK scheme. \end{cases} \tag{22}$$

Of particular note is that in Eq. (22), the constellation sizes are discrete, with their domains being $\{2,4,8,16,\ldots\}$. Considering QAM for example, the constellation size is generally larger than 2 (corresponding to PAM).

According to Eq. (17), the optimization problem can be distilled down to maximizing

$$\frac{R}{B} = \sum_{\eta=0}^{N_1-1}\sum_{\delta=0}^{N_2-1}(\omega_1\lambda_1 k_{1,\eta}+\omega_2\lambda_2 k_{2,\delta})\int\int_{D_{\eta,\delta}} p(\gamma_1)p(\gamma_2)d\gamma_1 d\gamma_2 \tag{23}$$

subject to

$$\begin{cases} \sum_{\eta=0}^{N_1-1}\sum_{\delta=0}^{N_2-1}\int\int_{D_{\eta,\delta}} \frac{S_{\eta\delta}(\gamma_1,\gamma_2)}{\bar{S}} p(\gamma_1)p(\gamma_2)d\gamma_1 d\gamma_2 = 1 \\ D_{\eta,\delta} \bigcap D_{\eta',\delta'} = \phi \\ \bigcup_\eta \bigcup_\delta D_{\eta,\delta} = \mathbb{R}^2, \end{cases} \tag{24}$$

where $D_{\eta,\delta}$ and $D_{\eta',\delta'}$ denote the different regions corresponding to the different transmit rates of $k_{1,\eta}$, $k_{2,\delta}$ and $k_{1,\eta'}$, $k_{2,\delta'}$.

To find the optimal fading-magnitude divisions for each destination node, we may also formulate the Lagrangian with the aid of the KKT conditions. However, the shape of $D_{\eta,\delta}$ obeys arbitrary quadrilaterals, therefore the discrete-rate optimization problem becomes excessively complex to be solved with the aid of general optimization methods. Inspired by the basic set-partition algorithm of [15], without changing the nature of the problem, we make some adjustments for our problem by restricting the fading-magnitude regions into rectangular areas (Fig. 3 shows the schematic of this version). In each rectangular area, we use the constellation sizes $M_{1,\eta}, \eta \in \mathbb{N}$ for DN1 and $M_{1,\delta}, \delta \in \mathbb{N}$ for DN2, which determine the attainable transmission rates.

$$\begin{aligned} J\left[\upsilon^*, D, \gamma_1, \gamma_2, S(\gamma_1,\gamma_2)\right] = &\int\int_D R\left[\gamma_1,\gamma_2,S(\gamma_1,\gamma_2)\right]d\gamma_1 d\gamma_2 + \upsilon^*\left(\bar{S} - \int\int_D S(\gamma_1,\gamma_2)p(\gamma_1)p(\gamma_2)d\gamma_1 d\gamma_2\right) \\ &+ \int\int_D \mu^* S(\gamma_1,\gamma_2)p(\gamma_1)p(\gamma_2)d\gamma_1 d\gamma_2 \end{aligned} \tag{18}$$

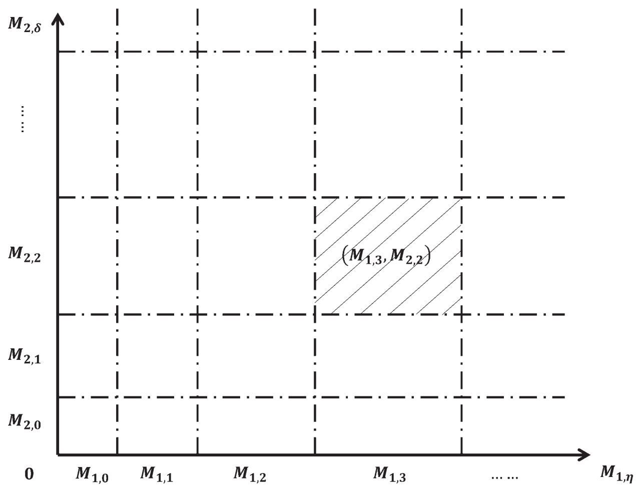

Fig. 3. Schematic of rectangular areas.

According to our adjusted method, the optimization problem can be simplified to that of maximizing

$$\frac{R}{B}=\sum_{\eta=0}^{N_1-1}\sum_{\delta=0}^{N_2-1}(\omega_1 k_{1,\eta}+\omega_2 k_{2,\delta})\int_{\gamma_{1,\eta-1}}^{\gamma_{1,\eta}} p(\gamma_1)d\gamma_1 \int_{\gamma_{2,\delta-1}}^{\gamma_{2,\delta}} p(\gamma_2)d\gamma_2 \tag{25}$$

subject to

$$\begin{cases}\sum_{\eta=0}^{N_1-1}\sum_{\delta=0}^{N_2-1}\int_{\gamma_{1,\eta-1}}^{\gamma_{1,\eta}}\int_{\gamma_{2,\delta-1}}^{\gamma_{2,\delta}}\frac{S_{\eta\delta}(\gamma_1,\gamma_2)}{\bar{S}}p(\gamma_1)p(\gamma_2)d\gamma_1 d\gamma_2=1\\ 0<\gamma_{1,0}<\ldots<\gamma_{1,\eta-1}<\gamma_{1,\eta}<\ldots<\gamma_{1,N_1-1}\\ 0<\gamma_{2,0}<\ldots<\gamma_{2,\delta-1}<\gamma_{2,\delta}<\ldots<\gamma_{2,N_2-1},\end{cases} \tag{26}$$

where $\gamma_{1,\eta}$ and $\gamma_{1,j}$ denote the rectangular fading region boundaries, and again, $k_{1,\eta}$, $k_{2,\delta}$, $p(\gamma_1)$, $p(\gamma_2)$, ω_1 and ω_2 are derived previously.

The corresponding power adaptation policy is the same as that of Eq. (21). Upon substituting Eq. (21) into Eq. (26), we may rewrite the power constraint as Eq. (27), shown at the bottom of the page. An intuitive interpretation of Eq. (27) is as follows. Throughout the entire fading-magnitude region, given γ_1, γ_2 and $S_{\eta\delta}(\gamma_1,\gamma_2)$, the discrete transmit rates destined for DN1 and DN2 cannot reach their optimal match with the same power at the same time. However, in the context of joint optimization, Eq. (21) facilitates that at least one of the equalities is satisfied in Eq. (20), which implies that if one of the user's rate and power achieves the optimal match,[2] the other user will have a rate determined by the maximum constellation size it can reach. In other words, it is highly likely that for the other DL user, the power will be higher than that required by the user's modulation mode at this moment. Intuitively, according to our proposed power allocation policy, the optimization target is that of maximizing the pair of users' weighted sum rate. Therefore, the index of the particular user that reaches its optimal match with the available power depends mainly on its weight coefficient and instantaneous SNR. In other words, the identifier of the specific user that reaches its optimal power and rate match is ultimately determined by its contribution to the sum rate.

Based on the above discussions, we may obtain the optimal region partitions $R_{1,\eta}=[\gamma_{1,\eta-1},\gamma_{1,\eta}),\eta=0,\ldots,N_1-1$ and $R_{2,\delta}=[\gamma_{2,\delta-1},\gamma_{2,\delta}),\delta=0,\ldots,N_2-1$, which are jointly determined by the average power constraint and the fading distributions. There is no closed-form solution to this kind of problem [15]. However, similarly to the approach of [15], we conceive a numerical search algorithm *with low complexity* for finding the optimal boundaries[3] $R_{1,\eta}$ and $R_{2,\delta}$. This may require a large amount of calculations. However, once the optimal boundaries have been found, they can be used without real-time calculations.

C. *Continuous-Rate Adaptive M-ary NC-QAM/PSK*

According to the optimization problem formulated in Subsection A, our continuous-rate adaptive NC-QAM and the concept of generalized adaptive NCM will be investigated in this subsection. In contrast to the information theoretic discussion of [18], the proposed continuous-rate adaptive NCM schemes are based on BER bounds. More particularly, the SNR-loss imposed by adaptive NC-QAM will be discussed in the context of the associated BER expressions. For PSK and other M-ary modulations, which obey the BER-bound of (11), a unified solution is presented, which relies on channel prediction.

1) Continuous-Rate Adaptation for NC-QAM: As discussed in Subsection A, a tight BER bound is given by Eq. (11). For NC-QAM, the maximum constellation size capable of meeting the target P_{b_i} is given by Eq. (14). Let $c_1=0.2$, $c_2=1.5$, $c_3=1$ and $c_4=1$ when $M_i\geq 4$ and $0\leq\gamma_i\leq 30$ dB [23]. For our continuous-rate scheme, the pair of inequalities in Eq. (14) are capable of simultaneously meeting the equality conditions. We then have

$$\begin{cases}M_1(\gamma_1)=1+K_1\lambda_1\gamma_1\frac{S(\gamma_1,\gamma_2)}{\bar{S}}\\ M_2(\gamma_2)=1+K_2\lambda_2\gamma_2\frac{S(\gamma_1,\gamma_2)}{\bar{S}},\end{cases} \tag{28}$$

where $K_i=-1.5/\ln(5P_{b_i}), i=1,2$.

According to Eq. (16), the rate function of jointly-optimal NC-QAM may be formulated as

$$R\left[\gamma_i,S(\gamma_1,\gamma_2)\right]=\sum_{i=1}^{2}\omega_i\log_2\left(1+K_i\lambda_i\gamma_i\frac{S(\gamma_1,\gamma_2)}{\bar{S}}\right),\ i=1,2. \tag{29}$$

[2]Here, the optimal match implies that the transmit power is the one which happens to be the power that a specific modulation mode requires.

[3]The optimal boundaries are the optimal channel state thresholds corresponding to the different modulation modes.

$$\sum_{\eta=0}^{N_1-1}\sum_{\delta=0}^{N_2-1}\int_{\gamma_{1,\eta-1}}^{\gamma_{1,\eta}}\int_{\gamma_{2,\delta-1}}^{\gamma_{2,\delta}}\max\left\{\frac{M_{1,\eta}-c_4}{\lambda_1 K_1\gamma_1},\frac{M_{2,\delta}-c_4}{\lambda_2 K_2\gamma_2},0\right\}p(\gamma_1)p(\gamma_2)d\gamma_1 d\gamma_2=1 \tag{27}$$

Again, the SNR-loss imposed by NC-QAM was quantified in terms of a so-called 'SNR-loss coefficient λ' in [8], which will now be considered in the context of Eq. (13). Specifically, we found that for the larger constellation size of the two, there is no SNR-loss according to [8]. In other words, the SNR loss only exists for the specific destination node, which has the smaller constellation size. Furthermore, the SNR-loss decreases upon increasing the receiver-side SNR. Based on the above discussions, we treat the coefficients λ_1 and λ_2 as a pair of inequality constrains.

For fading channels, we substitute Eq. (29) into Eq. (17) and then reformulate the optimization problem by maximizing

$$\frac{R}{B}=\int_0^{\infty}\int_0^{\infty}\sum_{i=1}^{2}\omega_i\log_2\left(1+K_i\lambda_i\gamma_i\frac{S(\gamma_1,\gamma_2)}{\bar{S}}\right)p(\gamma_1)p(\gamma_2)d\gamma_1 d\gamma_2 \tag{30}$$

subject to

$$\begin{cases}\int_0^{\infty}\int_0^{\infty} S(\gamma_1,\gamma_2)p(\gamma_1)p(\gamma_2)d\gamma_1 d\gamma_2=\bar{S}\\ S(\gamma_1,\gamma_2)\geq 0\\ \lambda_1\left(1-\frac{1}{(1+K_2\gamma_2\lambda_2 S(\gamma_1,\gamma_2/\bar{S})}\right)\leq 1-\frac{1}{(1+K_1\gamma_1\lambda_1 S(\gamma_1,\gamma_2)/\bar{S})}\\ \lambda_2\left(1-\frac{1}{(1+K_1\gamma_1\lambda_1 S(\gamma_1,\gamma_2)/\bar{S})}\right)\leq 1-\frac{1}{(1+K_2\gamma_2\lambda_2 S(\gamma_1,\gamma_2)/\bar{S})}\\ \lambda_1\leq 1\\ \lambda_2\leq 1,\end{cases} \tag{31}$$

$$\lambda_i=\min\left(1,\frac{1-M_i(\gamma_i)^{-1}}{1-M_{3-i}(\gamma_{3-i})^{-1}}\right),\quad i=1,2, \tag{32}$$

where ω_1, ω_2, $\bar{S}$, $S(\gamma_1,\gamma_2)$, γ_i, $\overline{\gamma_i}$, $p(\gamma_i)$ and P_{b_i} are defined as in the previous subsection.

Upon substituting Eq. (32) into Eq. (30), we arrive at a challenging problem, which is difficult to solve using general mathematical tools. When considering the SNR-loss coefficients, we will simplify our discussions by setting an upper bound and a lower bound for λ_i.

The upper bound readily emerges by letting $\lambda_1=\lambda_2=1$, which means that there is no SNR-loss. As to the lower bound, we first set $\lambda_1=\lambda_2=\lambda^*$, which results in:

$$\begin{cases}M_1(\gamma_1)=1+K_1\lambda^*\gamma_1\frac{S(\gamma_1,\gamma_2)}{\bar{S}}\\ M_2(\gamma_2)=1+K_2\lambda^*\gamma_2\frac{S(\gamma_1,\gamma_2)}{\bar{S}}.\end{cases} \tag{33}$$

We now have to discuss different cases for Eq. (33). If we consider $K_1\gamma_1\geq K_2\gamma_2$ first, then we have $M_1(\gamma_1)\geq M_2(\gamma_2)$. According to Eq. (13), the SNR-loss coefficients λ^* now becomes

$$\begin{aligned}\lambda^*&=\frac{1-\left(1+K_2\lambda^*\gamma_2\frac{S(\gamma_1,\gamma_2)}{\bar{S}}\right)^{-1}}{1-\left(1+K_1\lambda^*\gamma_1\frac{S(\gamma_1,\gamma_2)}{\bar{S}}\right)^{-1}}\\ &>1-\left(1+K_2\lambda^*\gamma_2\frac{S(\gamma_1,\gamma_2)}{\bar{S}}\right)^{-1}.\end{aligned} \tag{34}$$

Since the constellation size of MQAM is larger than 2, we then set the lower bound by letting $M_1(\gamma_1)\geq M_2(\gamma_2)\geq 2$, which implies that we may have

$$\lambda^*>1-\left(1+K_2\lambda^*\gamma_2\frac{S(\gamma_1,\gamma_2)}{\bar{S}}\right)^{-1}=\frac{1}{2}. \tag{35}$$

For the scenario of $K_1\gamma_1\leq K_2\gamma_2$, we may get result similar to Eq. (35). Since the SNR-loss decreases upon increasing the constellation size, it is reasonable to set a lower bound by letting $\lambda^*=0.5$. Hence we have found both a lower and an upper bound for the SNR-loss coefficients.

Let us now discuss the corresponding solutions for adaptive NC-QAM. Let us commence by considering the simple case of $\lambda_1=\lambda_2=1$, for the target BER functions associated with $K_1=K_2=K$ and the weight factors of $\omega_1=\omega_2=0.5$. To find the optimal power allocation $S(\gamma_1,\gamma_2)$, we substitute $\lambda_1=\lambda_2=1$, as well as $K_1=K_2=K$ into Eq. (30) and Eq. (31). Then we may rewrite Eq. (18) as

$$\begin{aligned}&J\left[S(\gamma_1,\gamma_2)\right]\\ &=\int_0^{\infty}\int_0^{\infty}\sum_{i=1}^{2}\omega_i\log_2\left(1+K\gamma_i\frac{S(\gamma_1,\gamma_2)}{\bar{S}}\right)p(\gamma_1)p(\gamma_2)d\gamma_1 d\gamma_2\\ &\quad+\upsilon^*\left(\bar{S}-\int_0^{\infty}\int_0^{\infty}S(\gamma_1,\gamma_2)p(\gamma_1)p(\gamma_2)d\gamma_1 d\gamma_2\right)\\ &\quad+\int_0^{\infty}\int_0^{\infty}\mu^* S(\gamma_1,\gamma_2)p(\gamma_1)p(\gamma_2)d\gamma_1 d\gamma_2.\end{aligned} \tag{36}$$

Upon differentiating the Lagrangian and setting the resultant derivative to zero, we arrive at:

$$\frac{\partial J\left[S(\gamma_1,\gamma_2)\right]}{\partial S(\gamma_1,\gamma_2)}=0,\ \frac{\partial J(\upsilon^*)}{\partial\upsilon^*}=0, \tag{37}$$

yielding:

$$\begin{cases}\left[\sum_{i=1}^{2}\omega_i\left(\frac{1/\ln 2}{1+K\gamma_i\frac{S(\gamma_1,\gamma_2)}{\bar{S}}}\right)\frac{K\gamma_i}{\bar{S}}-\upsilon^*+\mu^*\right]p(\gamma_1)p(\gamma_2)=0\\ \mu^* S(\gamma_1,\gamma_2)=0\\ S(\gamma_1,\gamma_2)\geq 0\\ \mu^*\geq 0.\end{cases} \tag{38}$$

Solving Eq. (38) for $S(\gamma_1,\gamma_2)$ under the relevant power constraint yields the complementary slack condition υ^* (see bottom of the next page)[4] and the power adaptation policy that maximizes Eq. (30), as seen in Eq. (39), shown at the bottom of the next page. Upon substituting the channel estimates and the power adaptation policy of Eq. (39) back into Eq. (30), we arrive at the jointly-optimized cutoff fade depth υ^*, below which the transmissions are disabled. Then the maximum spectral efficiency can be achieved for the parameters γ_1, γ_2, $p(\gamma_1)$,

[4]Firstly, when $\mu^*>0, S(\gamma_1,\gamma_2)=0$, we have $(\omega_1 K\gamma_1/\overline{S}\ln 2)+(\omega_2 K\gamma_2/\overline{S}\ln 2)-\upsilon^*+\mu^*=0\Rightarrow\upsilon^*>(\omega_1 K\gamma_1+\omega_2 K\gamma_2/\overline{S}\ln 2)$. Secondly, when $\mu^*=0, S(\gamma_1,\gamma_2)>0$, we have $\upsilon^*=(\omega_1 K\gamma_1/\overline{S}\ln 2(1+K\gamma_1(S(\gamma_1,\gamma_2)/\overline{S})))+(\omega_2 K\gamma_2/\overline{S}\ln 2(1+K\gamma_2(S(\gamma_1,\gamma_2)/\overline{S})))<(\omega_1 K\gamma_1+\omega_2 K\gamma_2/\overline{S}\ln 2)$. Finally, the critical value is classified into the first case. So we get the complementary slack condition υ^*.

$p(\gamma_2)$, ω_1, ω_2, P_{b_1} and P_{b_2}. For the lower bound of $\lambda_i = 0.5$, we may arrive at a similar expression.

What has been discussed above is a special case of MQAM, where the BER requirements at both DN1 and DN2 are the same and the SNR loss coefficients are $\lambda_i = 1$. In the following subsection we will extend our variable-rate, variable-power adaptation scheme to more general schemes, such as NC-PSK, where there is no SNR loss.

2) Continuous-Rate Adaptation for General M-ary Modulation: The variable-rate and variable-power techniques discussed above for MQAM can be applied to other M-ary modulations. For any modulation scheme having a BER expression similar to Eq. (11), the basic premises are the same. Both the transmit power and the constellation sizes are adapted for maintaining both target BERs of the DN1 and DN2, while maximizing the overall rates. Given the parameters of $\bar{S}$, $S(\gamma_1, \gamma_2)$, γ_i, $\overline{\gamma_i}$, $p(\gamma_i)$ and P_{b_i} in our system model, there is no SNR-loss in the BER expression of NC-PSK, therefore we let $\lambda_1 = \lambda_2 = 1$ for our adaptive NC-PSK scheme. Without loss of generality, the BER requirements of NC-PSK can be different, given K_1 and K_2 in Eq. (15). Using the same method as in the previous subsection, we arrive at the following more general power adaptation policy see Eq. (40), shown at the bottom of the page.

When considering MPSK relying on the BER bound of Eq. (9.49) in [23] for example, by substituting $c_1 = 0.05$, $c_2 = 6$, $c_3 = 1.9$, $c_4 = 1$, γ_i, $\overline{\gamma_i}$, $p(\gamma_i)$ and P_{b_i} into Eq. (15), we may find the best cutoff fade depth υ^*, which hence allows us to calculate the maximum achievable spectral efficiency for the conditions considered.

D. Continuous-Rate Discretization for Adaptive M-ary QAM/PSK

Based on our discussions of the continuous-rate adaptation scheme of Subsection C, in this subsection, we proposed another discrete-rate transmission scheme, which we refer to as the Continuous-Rate Discretization Algorithm of NC-QAM/PSK. In our following discussions we consider the SNR loss upper bound of $\lambda_1 = \lambda_2 = 1$ for MQAM.

We assume that the parameters of our continuous-rate scheme have already been calculated. The divisions of the fading-magnitude regions are the same as in Subsection B. The discrete sets of MQAM/MPSK transmission modes are $\mathcal{M}_1 = \{M_{1,0}, \ldots, M_{1,N_1-1}\}$, $\mathcal{M}_2 = \{M_{2,0}, \ldots, M_{2,N_2-1}\}$, with $M_{1,0} = 0$ and $M_{2,0} = 0$ implying no transmission. Let $M'_{1,\eta}$ and $M'_{2,\delta}$ denote the new rates corresponding to the continuous rates of M_1 and M_2, when they falls into specific fading-partitions. According to Eq. (17), the target problem now becomes that of calculating Eq. (41), shown at the bottom of the page, where $M'_{1,\eta}$ and $M'_{2,\delta}$ are obtained with the aid of Algorithm 1. Again, $\omega_1, \omega_2, \gamma_1, \gamma_2, p(\gamma_1), p(\gamma_2), P_{b_1}, P_{b_2}$ and $\overline{S}$ are all the same, as in the previous subsections.

Algorithm 1 Continuous Rate Discretization Algorithm

- Step 1) Calculate the corresponding parameters M_1, M_2, $S(\gamma_1, \gamma_2)$ and υ^* for given γ_1, γ_2 values in the context of our continuous-rate adaptive scheme.
- Step 2) Round M_1, M_2 down to the nearest integer constellation sizes of $M'_{1,\eta} \in \mathcal{M}_1, M'_{2,\delta} \in \mathcal{M}_2$ with $S(\gamma_1, \gamma_2)$ remaining unchanged.
- Step 3) Substitute $M'_{1,\eta}$, $M'_{2,\delta}$ into Eq. (41) and recalculate the spectral efficiency.

It is important to note that when we round the continuous-valued M_1, M_2 down to the nearest integers, the transmit power $S(\gamma_1, \gamma_2)$ remains unchanged. Additionally, letting $\lambda_1 = \lambda_2 = 1$ for MQAM implies that we ignore the SNR loss, which is indeed small enough to be neglected. Although this arrangement is not as beneficial as the scheme of Subsection B, the proposed design provides another feasible technique of realizing adaptive NC-QAM/PSK.

$$\frac{S(\gamma_1,\gamma_2)}{\bar{S}} = \begin{cases} \frac{1}{2}\sqrt{\left(\frac{1}{K\gamma_1}+\frac{1}{K\gamma_2}-\frac{1}{\upsilon^*\bar{S}\ln 2}\right)^2-\frac{4}{\upsilon^* K^2\gamma_1\gamma_2}\left(\upsilon^*-\frac{\omega_1 K\gamma_1+\omega_2 K\gamma_2}{\bar{S}\ln 2}\right)}+\frac{1}{2\upsilon^*\bar{S}\ln 2}-\frac{1}{2K\gamma_1}-\frac{1}{2K\gamma_2}, \upsilon^* < \frac{\omega_1 K\gamma_1+\omega_2 K\gamma_2}{\bar{S}\ln 2} \\ 0, \upsilon^* \geq \frac{\omega_1 K\gamma_1+\omega_2 K\gamma_2}{\bar{S}\ln 2} \end{cases} \tag{39}$$

$$\frac{S(\gamma_1,\gamma_2)}{\bar{S}} = \begin{cases} \frac{1}{2}\sqrt{\left(\frac{c_4}{K_1\gamma_1}+\frac{c_4}{K_2\gamma_2}-\frac{1}{\upsilon^* c_3\bar{S}\ln 2}\right)^2-\frac{4}{\upsilon^* K_1 K_2\gamma_1\gamma_2}\left(\upsilon^* c_4^2-\frac{\omega_1 c_4 K_1\gamma_1+\omega_2 c_4 K_2\gamma_2}{c_3\bar{S}\ln 2}\right)}+\frac{1}{2\upsilon^* c_3\bar{S}\ln 2}-\frac{c_4}{2K_1\gamma_1}-\frac{c_4}{2K_2\gamma_2}, \\ \upsilon^* < \frac{\omega_1 K_1\gamma_1+\omega_2 K_2\gamma_2}{c_3 c_4\bar{S}\ln 2} \\ 0, \upsilon^* \geq \frac{\omega_1 K_1\gamma_1+\omega_2 K_2\gamma_2}{c_3 c_4\bar{S}\ln 2} \end{cases} \tag{40}$$

$$\frac{R}{B} = \int_0^\infty \int_0^\infty \sum_{\eta=1}^{N_1-1} \sum_{\delta=1}^{N_2-1} \left[\frac{\omega_1}{c_3}\log_2\left(M'_{1,\eta}\right)+\frac{\omega_2}{c_3}\log_2\left(M'_{2,\delta}\right)\right] p(\gamma_1)p(\gamma_2)d\gamma_1 d\gamma_2 \tag{41}$$

TABLE I
SCENARIOS AND UNIFIED PARAMETERS FOR QAM

Scenarios	Rate and Power Strategies	System Model	Bound	BER	SNR loss	Unified Parameters
Scenario 1	AWGN Channel Capacity					
Scenario 2	Optimal Rate and Power Adaptation	Single-User	Shannon Bound			$p(\gamma_i)=\frac{1}{\overline{\gamma_i}}e^{-\gamma_i/\overline{\gamma_i}}, i=1,2.$
Scenario 3	Optimal Rate and Power Adaptation	DF-TWR				$\overline{S}=1$
Scenario 4	Optimal Rate and Constant Power	Single-User				$B=1$
Scenario 5	Optimal Rate and Power Adaptive MQAM	Single-User	BER Bound	$P_b=10^{-3}$		$\omega_1=\omega_2=0.5$
Scenario 6	Optimal Rate and Power Adaptive M-ary NC-QAM	DF-TWR		$P_{b_1}=P_{b_2}=10^{-3}$	$\lambda_1=\lambda_2=1$	$\gamma_i \in [0, 10*\overline{\gamma_i}], i=1,2$
Scenario 7	Optimal Rate and Power Adaptive M-ary NC-QAM	DF-TWR		$P_{b_1}=P_{b_2}=10^{-3}$	$\lambda_1=\lambda_2=0.5$	$\overline{\gamma_i}$={ 1,2,3,4,5,10,15,30,100,200,316}
Scenario 8	Optimal Rate and Constant Power	Single-User		$P_b=10^{-3}$		

TABLE II
SCENARIOS AND UNIFIED PARAMETERS FOR PSK

Scenarios	Rate and Power Strategies	System Model	Bound	BER	SNR loss	Unified Parameters
Scenario 1	AWGN Channel Capacity					
Scenario 2	Optimal Rate and Power Adaptation	Single-User	Shannon Bound			$p(\gamma_i)=\frac{1}{\overline{\gamma_i}}e^{-\gamma_i/\overline{\gamma_i}}, i=1,2.$
Scenario 3	Optimal Rate and Power Adaptation	DF-TWR				$\overline{S}=1,\ B=1$
Scenario 4	Optimal Rate and Constant Power	Single-User				$\omega_1=\omega_2=0.5$
Scenario 5	Optimal Rate and Power Adaptive MPSK	Single-User	BER Bound	$P_b=10^{-3}$		$\gamma_i \in [0, 10*\overline{\gamma_i}], i=1,2$
Scenario 6	Optimal Rate and Power Adaptive M-ary NC-PSK	DF-TWR		$P_{b_1}=P_{b_2}=10^{-3}$		$\overline{\gamma_i}$= {1,2,3,4,5,10,15,30,100,200,316}
Scenario 7	Optimal Rate and Constant Power	Single-User		$P_b=10^{-3}$		

IV. PERFORMANCE RESULTS

A basic fixed-rate of NC-QAM/PSK was proposed in [8], [9], which provides the basis of our adaptive transmission scheme. In this section, a range of representative numerical results are presented for validating our theoretical analysis. Our emphasis is on the spectral efficiency of variable-rate, variable-power NC-QAM/PSK. Furthermore, both the continuous-rate and discrete-rate adaptive NC-QAM/PSK schemes are compared to their respective benchmark schemes for demonstrating its potential. Specifically, we invoke the single-user adaptive MQAM/MPSK scheme of [15], [23] and the Shannon capacity based joint-optimization schemes [14], [18] as our benchmarks, which are described as Scenario 1–8 in Tables I and II.

The following assumptions will be exploited throughout our simulations. Let us focus our attention on Rayleigh fading channels, where the fading distributions are given by Eq. (10). The near-instantaneous SNR fluctuations are limited to a dynamic range, which was set to be 10 times the average SNR. The SNR-loss coefficient upper bounds of NC-QAM are set to $\lambda_1=\lambda_2=1$ (Scenario 6), while the lower bounds are set to $\lambda_1=\lambda_2=0.5$ (Scenario 7). For continuous-rate adaptive NC-QAM/PSK schemes, all the other parameters of Scenarios 1–8 are depicted in Tables I and II.

Figs. 4 and 5 also include the benchmarks of [14] (versus Scenarios 4 and 8), [15] (versus Scenarios 2 and 5), [18] (versus Scenario 3), as well as Eqs. (39) and (40) (versus Scenarios 6 or 7) derived for our MQAM/MPSK scheme as a function of the average received SNR for transmission over Rayleigh fading channels. The capacity of an AWGN channel (versus Scenario 1) is also shown as comparison for the same average power. Several observations are worth discussing. Firstly, our adaptive NC-QAM/PSK is capable of approaching both the

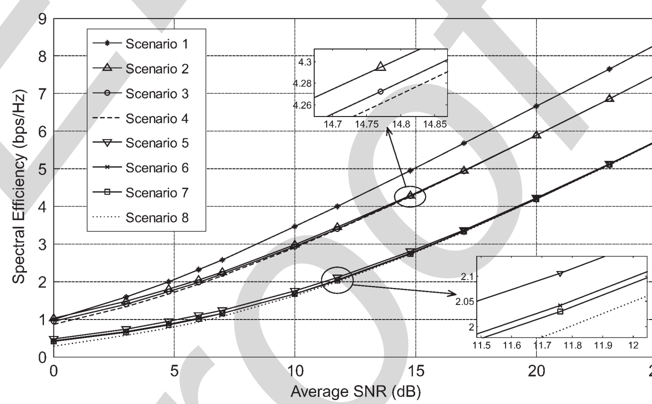

Fig. 4. Comparison of Scenarios 1–8 in terms of their spectral efficiency (QAM).

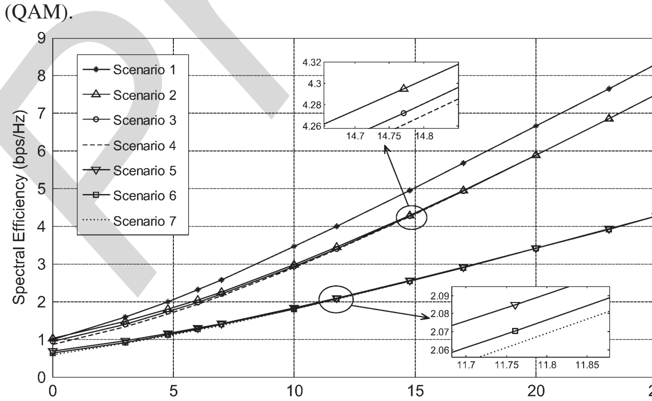

Fig. 5. Comparison of Scenarios 1–7 in terms of their spectral efficiency (PSK).

capacities of our proposed continuous-rate adaptive schemes, as well as of the schemes proposed in [18] and those of the single-user adaptation proposed in [15]. This is quite valuable, because we are supporting a bidirectional network-coded scenario.

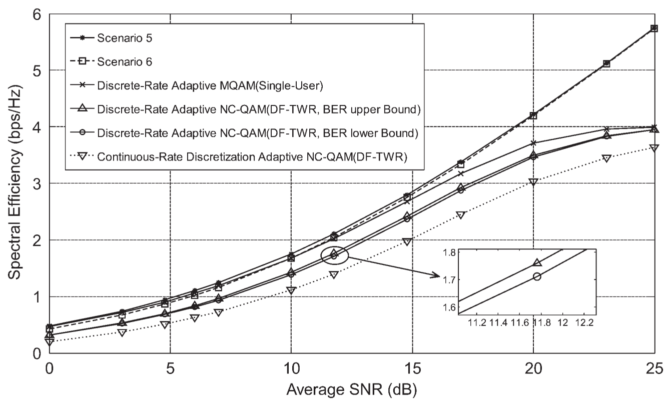

Fig. 6. Spectral efficiency of our continuous-rate adaptive NC-QAM, discrete-rate adaptive NC-QAM, continuous-rate discretization adaptive NC-QAM (Scenario 5, 6 of Fig. 4, $M = \{0, 2, 4, 16\}$).

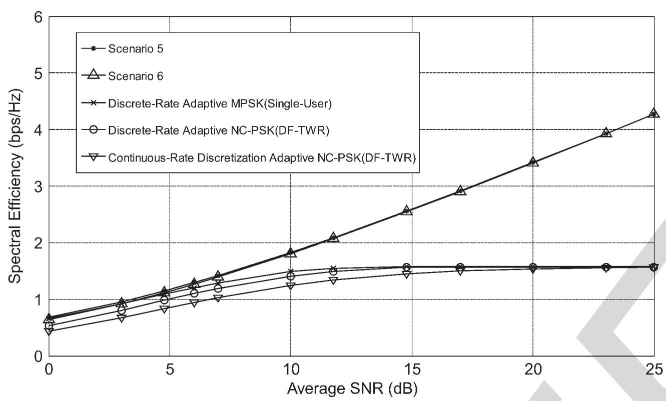

Fig. 7. Spectral efficiency of our continuous-rate adaptive NC-PSK, discrete-rate adaptive NC-PSK, continuous-rate discretization adaptive NC-PSK (Scenario 5, 6 of Fig. 5, $M = \{0, 2, 4, 8\}$).

Of particular note is in Fig. 4 that Eq. (39) relies on the upper bound of the SNR-loss coefficients, which were discussed in Section III. In Fig. 4 we also characterized NC-QAM relying on the SNR-loss lower bound associated with $\lambda_1 = \lambda_2 = 0.5$. The upper- and lower-bound curves are quite close to each other, which indicates that the impact of SNR-loss on the achievable spectral efficiency is small enough to be neglected. Secondly, both our schemes and the scheme proposed in [18] perform better than MQAM operating without power adaptation (versus Scenarios 8 and 7 in Figs. 4 and 5, respectively). Finally, upon increasing of the SNR, the discrepancy between our proposed schemes and the single-user adaptive schemes of [15] tends to narrow.

The continuous-rate discretization algorithm is now compared to the discrete-rate scheme proposed in Section III-B, using the same parameters of $\overline{\gamma_i} = [1, 2, 3, 4, 5, 10, 15, 30, 50, 100, 200, 316]$, $i = 1, 2$, $\gamma_i \in [0, 10 * \overline{\gamma_i}]$, $\overline{S} = 1$, $\omega = 0.5$, $P_{b_i} = 10^{-3}$, $B = 1$, and the Rayleigh distribution $p(\gamma_i)$ given by Eq. (10). We divide the dynamic range of the fading into four regions, and employ $\mathcal{M}_i = \{0, 2, 4, 16\}$, $i = 1, 2$ for MQAM and $\mathcal{M}_i = \{0, 2, 4, 8\}$, $i = 1, 2$ for MPSK. The SNR-loss parameters λ_i are given by Eq. (22) for MQAM and $\lambda_i = 1$ for MPSK.

Figs. 6 and 7 characterize the performance of our discrete-rate variable-power MQAM/MPSK scheme as well as of the adaptive single-user scheme of [15] (versus Scenario 5) and of the continuous-rate discretization algorithm of Section III-D. Both

TABLE III
RATE AND POWER ADAPTATION FOR MQAM (4 REGIONS)

$\gamma_{1,\eta} Range$	$\gamma_{2,\delta} Range$	M_1	M_2	$S_{\eta\delta}(\gamma_1, \gamma_2)/\overline{S}$
$0 \leq \gamma_1 \leq 1.3$	$0 \leq \gamma_2 \leq 1.3$	0	0	0
	$1.3 \leq \gamma_2 \leq 3.2$	0	2	$\max\{0, \frac{1}{K\gamma_2}\}$
	$3.2 \leq \gamma_2 \leq 6.0$	0	4	$\max\{0, \frac{3}{K\gamma_2}\}$
	$6.0 \leq \gamma_2 \leq 10$	0	16	$\max\{0, \frac{7}{K\gamma_2}\}$
$1.3 \leq \gamma_1 \leq 3.2$	$0 \leq \gamma_2 \leq 1.3$	2	0	$\max\{\frac{1}{K\gamma_1}, 0\}$
	$1.3 \leq \gamma_2 \leq 3.2$	2	2	$\max\{\frac{1}{K\gamma_1}, \frac{1}{K\gamma_2}\}$
	$3.2 \leq \gamma_2 \leq 6.0$	2	4	$\max\{\frac{1}{(2/3)K\gamma_1}, \frac{3}{K\gamma_2}\}$
	$6.0 \leq \gamma_2 \leq 10$	2	16	$\max\{\frac{1}{(8/15)K\gamma_1}, \frac{15}{K\gamma_2}\}$
...	...	...	...	...
$6.0 \leq \gamma_1 \leq 10$	$3.2 \leq \gamma_2 \leq 6.0$	16	4	$\max\{\frac{15}{K\gamma_1}, \frac{3}{(4/5)K\gamma_2}\}$
$6.0 \leq \gamma_1 \leq 10$	$6.0 \leq \gamma_2 \leq 10$	16	16	$\max\{\frac{15}{K\gamma_1}, \frac{15}{K\gamma_2}\}$

TABLE IV
RATE AND POWER ADAPTATION FOR MPSK (4 REGIONS)

$\gamma_{1,\eta} Range$	$\gamma_{2,\delta} Range$	M_1	M_2	$S_{\eta\delta}(\gamma_1, \gamma_2)/\overline{S}$
$0 \leq \gamma_1 \leq 0.5$	$0 \leq \gamma_2 \leq 0.5$	0	0	0
	$0.5 \leq \gamma_2 \leq 1.1$	0	2	$\max\{0, \frac{1}{K\gamma_2}\}$
	$1.1 \leq \gamma_2 \leq 2.5$	0	4	$\max\{0, \frac{3}{K\gamma_2}\}$
	$2.5 \leq \gamma_2 \leq 10$	0	8	$\max\{0, \frac{7}{K\gamma_2}\}$
$0.5 \leq \gamma_1 \leq 1.1$	$0 \leq \gamma_2 \leq 0.5$	2	0	$\max\{\frac{1}{K\gamma_1}, 0\}$
	$0.5 \leq \gamma_2 \leq 1.1$	2	2	$\max\{\frac{1}{K\gamma_1}, \frac{1}{K\gamma_2}\}$
	$1.1 \leq \gamma_2 \leq 2.5$	2	4	$\max\{\frac{1}{K\gamma_1}, \frac{3}{K\gamma_2}\}$
	$2.5 \leq \gamma_2 \leq 10$	2	8	$\max\{\frac{1}{K\gamma_1}, \frac{7}{K\gamma_2}\}$
...	...	...	...	...
$2.5 \leq \gamma_1 \leq 10$	$1.1 \leq \gamma_2 \leq 2.5$	8	4	$\max\{\frac{7}{K\gamma_1}, \frac{7}{K\gamma_2}\}$
$2.5 \leq \gamma_1 \leq 10$	$2.5 \leq \gamma_2 \leq 10$	8	8	$\max\{\frac{7}{K\gamma_1}, \frac{7}{K\gamma_2}\}$

Figs. 6 and 7 show that the performance of our discrete-rate schemes approaches that of the adaptive single-user MQAM/MPSK schemes proposed in [15], despite the more challenging scenario of supporting bidirectional NC. According to Fig. 4, the proposed discrete-rate schemes exhibit a better performance than the scheme operating without power adaptation. Compared to the continuous-rate discretization algorithm, the discrete-rate continuous-power scheme proposed in Section III-B performs better. Additionally, it is important to note that in Fig. 6 we characterize the adaptive MQAM algorithm without considering the SNR-loss λ_i. Compared to adaptive MQAM taking into consideration the SNR-loss, the two curves are close, which indicates that the SNR-loss of the discrete-rate scheme is small enough to be ignored. Our simulation results also indicate that the gaps between our proposed schemes, the continuous-rate discretization algorithm and the adaptive single-user methods of [15] tend to decrease upon increasing of the average SNRs. Moreover, increasing the number N_i of discrete signal constellations yields a

TABLE V
PERFORMANCE COMPARISON OF CONTINUOUS-RATE AND DISCRETE-RATE SCHEMES (QAM)

Rate(bps/Hz)	$\overline{\gamma_i}$=1	$\overline{\gamma_i}$=2	$\overline{\gamma_i}$=3	$\overline{\gamma_i}$=4	$\overline{\gamma_i}$=5	$\overline{\gamma_i}$=10	$\overline{\gamma_i}$=15	$\overline{\gamma_i}$=30	$\overline{\gamma_i}$=50	$\overline{\gamma_i}$=100	$\overline{\gamma_i}$=200	$\overline{\gamma_i}$=316
Single-User Continuous Adaptation (Shannon bound)	0.4836	0.7421	0.9384	1.1012	1.2401	1.7519	2.1064	2.8005	3.3747	4.2215	5.1249	5.7434
DF-TWR Continuous Adaptation	0.4235	0.6702	0.8620	1.0226	1.1624	1.6804	2.0420	2.7517	3.3377	4.1978	5.1112	5.7338
Single-User Discrete-Rate Adaptive MQAM	0.4679	0.7158	0.9024	1.0558	1.1878	1.6786	2.0220	2.6809	3.1719	3.7060	3.9572	3.9951
DF-TWR Discrete-Rate Adaptive NC-QAM(SNR-loss upper bound)	0.3207	0.5281	0.6949	0.8375	0.9616	1.4274	1.7597	2.4193	2.9279	3.4989	3.8451	3.9526
DF-TWR Discrete-Rate Adaptive NC-QAM(SNR-loss lower bound)	0.3181	0.5210	0.6816	0.8171	0.9357	1.3857	1.7113	2.3606	2.8671	3.4587	3.8316	3.9485
Continuous-Rate Discretization Adaptive NC-QAM	0.1967	0.3667	0.5078	0.6275	0.7315	1.1149	1.3910	1.9717	2.4489	3.0335	3.4521	3.6356

better match with the continuous-rate adaptation scheme, hence resulting in a higher spectral efficiency.

Let us now conclude by considering both the power-allocation and rate-adaptation policy for a specific scenario, using the parameters of $\overline{\gamma_i} = 1, i = 1, 2, \gamma_i \in [0, 10], w_i = 0.5$, $P_{b_i} = 10^{-3}$, $\overline{S} = 1$, $B = 1$, $\mathcal{M}_i = \{0, 2, 4, 16\}$ for MQAM and $\mathcal{M}_i = \{0, 2, 4, 8\}$ for MPSK. The SNR-loss coefficients λ_i are given by Eq. (22) for MQAM and $\lambda_i = 1$ for MPSK.

In Table III we summarize the constellation sizes and power adaptation policies as functions of γ_1 and γ_2 for four fading regions corresponding to four MQAM/MPSK adaptive strategies. Upon solving Eqs. (25) and (27) we arrive at the corresponding switching thresholds divisions for MQAM as $R_1 = [0, 1.3, 3.2, 6.0, 10]$, $R_2 = [0, 1.3, 3.2, 6.0, 10]$, which are required for practical use. The corresponding maximum rate is 0.3207 bps/Hz. Similarly, Table IV characterizes the discrete-rate adaption scheme for MPSK under the same conditions as for MQAM, where we have $R_1 = [0, 0.5, 1.1, 2.5, 10]$, $R_2 = [0, 0.5, 1.1, 2.5, 10]$. The corresponding maximum rate is 0.5375 bps/Hz.

In Table V we tabulate the concrete numerical values of spectral efficiency for the Scenarios 1–8 of Fig. 6, which well support our conclusions.

V. CONCLUSION

In this paper, we developed an asymmetric adaptive transmission design for DF-TWR, which combines network coding with near-instantaneously adaptive modulation that adapts to the channel variations. The main emphasis of this design is on practical adaptive NCM, therefore our study was focused on discrete-rate adaptation schemes. Our simulation results demonstrated that the proposed variable-rate, variable-power NC-QAM/PSK DF-TWR schemes are capable of obtaining a higher spectral efficiency compared to the benchmark scheme operating without power adaptation. Finally, we demonstrated that the impact of SNR-loss on the achievable spectral efficiency is sufficiently low to be neglected.

APPENDIX
SNR-LOSS IMPOSED BY NC-QAM

For NC-QAM, the symbol to be transmitted to DN1 and DN2 will be circularly shifted by an amplitude of $2\sqrt{M_2}(a_i^I + ja_i^Q)d$ at the relay [8]. When we derive the symbol error rate (SER) of NC-QAM, intuitively, the SER of a circularly shifted M_i-ary QAM constellation is identical to that of the original M_i-ary QAM for the same minimum symbol distance. By recalling Eq. (3), Eq. (5) and that $a_i^I, a_i^Q \in \mathcal{A}_i$, we have $d_1 = (\sqrt{M_2}/\sqrt{M_1})d$ and $d_2 = d$. Let us insert d_1 and d_2 into Eq. (42) and introduce the M_1- and M_2-dependent coefficient of $\lambda_i = (1 - M_i^{-1}/1 - M_2^{-1}), M_2 > M_1$:

$$P_i = \frac{4(\sqrt{M_i} - 1)}{\sqrt{M_i}} Q\left(\sqrt{\frac{|h_i|^2 d_i^2}{N_0/2}}\right), \tag{42}$$

where P_i denotes the SER of the relay-DN1 and relay-DN2 links. We may thus arrive at the unified SER expressions of NC-QAM, given by

$$P_i = \frac{4(\sqrt{M_i} - 1)}{\sqrt{M_i}} Q\left(\sqrt{\frac{1.5\lambda_i\gamma_i}{M_i - 1}}\right). \tag{43}$$

According to the above analysis, for $M_2 > M_1$, we have $\lambda_1 = 1$ and $\lambda_2 < 1$, which implies imposing an SNR loss for the relay-DN1 link that remains constant across the entire SNR range. The reason for this SNR loss at the receiver of DN1 can be stated as follows. Since QAM is regarded as a pair of orthogonal signals PAM, we may simply focus our discussions on the I component. Given a_2^I, the legitimate symbols at the receiver of DN1 have a non-zero mean of

$$d\left[2\sqrt{M_2}\left(a_2^I \bmod \frac{1}{\sqrt{M_1}}\right) + 1 - \frac{\sqrt{M_2}}{\sqrt{M_1}}\right]. \tag{44}$$

In contrast to the classic zero-mean $\sqrt{M_1}$-ary PAM, the DC bias of such a circularly shifted $\sqrt{M_1}$-ary PAM constellation will result in some extra energy consumption, which therefore results in the above-mentioned SNR loss.

REFERENCES

[1] S.-Y. Li, R. W. Yeung, and N. Cai, "Linear network coding," *IEEE Trans. Inf. Theory.*, vol. 49, no. 2, pp. 371–381, Feb. 2003.
[2] Y. Wu, P. A. Chou, and S.-Y. Kung, "Information exchange in wireless networks with network coding and physical-layer broadcast," Microsoft Research, Redmond, WA, USA, Tech. Rep. MSR-TR-2004, 2004.
[3] Y. Wu, "Broadcasting when receivers know some messages *a priori*," in *Proc. IEEE ISIT*, Nice, France, Jun. 2007, pp. 1141–1145.
[4] L.-L. Xie, "Network coding and random binning for multi-user channels," in *Proc. 10th Can. Workshop Inf. Theory*, 2007, pp. 85–88.

[5] W. Chen, K. B. Letaief, and Z. Cao, "A cross layer method for interference cancellation and network coding in wireless networks," in *Proc. IEEE ICC*, Istanbul, Turkey, Jun. 2006, pp. 3693–3698.

[6] R. Y. Kim and Y. Y. Kim, "Symbol-level random network coded cooperation with hierarchical modulation in relay communication," *IEEE Trans. Consum. Electron.*, vol. 55, no. 3, pp. 1280–1285, Aug. 2009.

[7] J. M. Park, S.-L. Kim, and J. Choi, "Hierarchically modulated network coding for asymmetric two-way relay systems," *IEEE Trans. Veh. Technol.*, vol. 59, no. 5, pp. 2179–2184, Jun. 2010.

[8] W. Chen, Z. Cao, and L. Hanzo, "Maximum Euclidean distance network coded modulation for asymmetric decode-and-forward two-way relaying," *IET Commun.*, vol. 7, no. 10, pp. 2179–2184, Jul. 2013.

[9] W. Chen, L. Hanzo, and Z. Cao, "Network coded modulation for two-way relaying," in *Proc. IEEE WCNC*, Cancun, Mexico, Mar. 2011, pp. 1765–1770.

[10] J. Torrance and L. Hanzo, "Optimisation of switching levels for adaptive modulation in slow Rayleigh fading," *Electron. Lett.*, vol. 32, no. 13, pp. 1167–1169, Jun. 1996.

[11] L. Hanzo, C. H. Wong, and M.-S. Yee, *Adaptive Wireless Transceivers: Turbo-Coded, Turbo-Equalised and Space-Time Coded TDMA, CDMA and OFDM Systems*. Hoboken, NJ, USA: Wiley, 2002.

[12] L. Hanzo, S. X. Ng, W. Webb, and T. Keller, *Quadrature Amplitude Modulation: From Basics to Adaptive Trellis-Coded, Turbo-Equalised and Space-Time Coded OFDM, CDMA and MC-CDMA Systems*. Hoboken, NJ, USA: Wiley, 2004.

[13] S. T. Chung and A. J. Goldsmith, "Degrees of freedom in adaptive modulation: A unified view," *IEEE Trans. Commun.*, vol. 49, no. 9, pp. 1561–1571, Sep. 2001.

[14] A. J. Goldsmith and P. P. Varaiya, "Capacity of fading channels with channel side information," *IEEE Trans. Inf. Theory*, vol. 43, no. 6, pp. 1986–1992, Nov. 1997.

[15] A. J. Goldsmith and S.-G. Chua, "Variable-rate variable-power MQAM for fading channels," *IEEE Trans. Commun.*, vol. 45, no. 10, pp. 1218–1230, Oct. 1997.

[16] B. Choi and L. Hanzo, "Optimum mode-switching-assisted constant-power single-and multicarrier adaptive modulation," *IEEE Trans. Veh. Technol.*, vol. 52, no. 3, pp. 536–560, May 2003.

[17] Q. Liu, S. Zhou, and G. B. Giannakis, "Cross-layer combining of adaptive modulation and coding with truncated ARQ over wireless links," *IEEE Trans. Wireless Commun.*, vol. 3, no. 5, pp. 1746–1755, Sep. 2004.

[18] X. Chen and W. Chen, "Capacity of the broadcasting phase of time-varying two-way relaying," in *Proc. IEEE IWS*, Beijing, China, Apr. 2013, pp. 1–4.

[19] R. O. Afolabi, A. Dadlani, and K. Kim, "Multicast scheduling and resource allocation algorithms for OFDMA-based systems: A survey," *IEEE Commun. Surveys Tuts.*, vol. 15, no. 1, pp. 240–254, 2013.

[20] J. Vella and S. Zammit, "A survey of multicasting over wireless access networks," *IEEE Commun. Surveys Tuts.*, vol. 15, no. 2, pp. 718–753, 2013.

[21] J. Liu, W. Chen, Z. Cao, and K. B. Letaief, "Dynamic power and subcarrier allocation for OFDMA-based wireless multicast systems," in *Proc. IEEE ICC*, Beijing, China, May 2008, pp. 2607–2611.

[22] J. Yuan and K. L. Huang, "Adaptive modulation for MIMO broadcast channels," presented at the *International Conf. Signal Processing Communication Systems*, Gold Coast, Qld, Australia, Dec. 2012, Proc. ICSPCS'07.

[23] A. Goldsmith, *Wireless Communications*. Cambridge, U.K.: Cambridge Univ. Press, 2005.

[24] M. K. Simon and M.-S. Alouini, *Digital Communication Over Fading Channels*. New York, NY, USA: Wiley, 2005.

AQ1

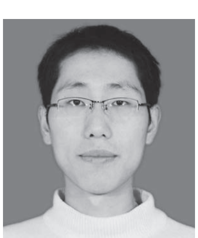

Yanping Yang (S'XX) received the B.S. degree in automation and the M.S. degree in electronic engineering from Xidian University, Xi'an China, in 2008, and 2013, respectively. He is currently studying in the Department of Electronic Engineering, Tsinghua University, Beijing, China. He is pursuing the Ph.D. degree in National Digital Switching System Engineering and Technological R&D Center, Zhengzhou, China.

His research interests include wireless communications and cognitive radio networks. He currently serves as a Reviewer for the IEEE Wireless Communications Letters, the IEEE ICCS, and the IEEE ATC.

Wei Chen (S'05–M'07–SM'13) received the B.S. and Ph.D. degrees in electronic engineering (both with the highest honors) from Tsinghua University, Beijing, China, in 2002, and 2007, respectively. From 2005 to 2007, he was also a visiting research staff member in the Hong Kong University of Science and Technology (HKUST). Since July 2007, he has been with Department of Electronic Engineering, Tsinghua University, where he is a Full Professor and the Chair of department teaching committee. He visited the University of Southampton, UK, from June 2010 to Sept. 2010, and Telecom ParisTech, France, from June 2014 to Sept. 2014. Dr. Chen is a 973 Youth Project chief scientist and a national young and middle-aged leader for science and technology innovation. He is also supported by the NSFC excellent young investigator project, new century talent program of Ministry of Education, Beijing nova program, and 100 fundamental research talents program of Tsinghua University (also known as 221 talents Program).

His research interests are in areas of wireless communications, information theory, and applied optimizations. He serves as Editor for IEEE TRANSACTIONS ON EDUCATION, IEEE WIRELESS COMMUNICATIONS LETTERS, and China Communications, as a Vice Director of youth committee of China Institute of Communications. He served as a tutorial co-chair of the 2013 IEEE ICC, a TPC co-chair of 2011 Spring IEEE VTC, and symposium co-chairs for IEEE ICC, ICCC, and CCNC. He was the recipient of the First Prize of 14th Henry Fok Ying-Tung Young Faculty Award, the 2010 IEEE Comsoc Asia Pacific Board Best Young Researcher Award, the 2009 IEEE Marconi Prize Paper Award, the Best Paper Awards at IEEE ICC 2006, IEEE IWCLD 2007, and IEEE Smart Gird Com. 2012, the 2011 Tsinghua Raising Academic Star Award. Prof. Chen holds the honorary titles of Beijing excellent teacher and Beijing excellent young talent. He is the Champion of the first national young faculty teaching competition, and a winner of National May 1st Medal.

Ou Li received the Ph.D. degree from National Digital Switching System Engineering and Technological Research Center (NDSC), Zhengzhou, China, in 2001. He is currently a Professor at NDSC in China.

His primary research interests include wireless communication technology, wireless sensor network and cognitive radio networks.

Lajos Hanzo (F'XX) received the degree in electronics in 1976 and his doctorate in 1983. In 2009 he was awarded the honorary doctorate "Doctor Honoris Causa" by the Technical University of Budapest. During his 38-year career in telecommunications he has held various research and academic posts in Hungary, Germany and the UK. Since 1986 he has been with the School of Electronics and Computer Science, University of Southampton, UK, where he holds the chair in telecommunications. He has successfully supervised about 100 PhD students, co-authored 20 John Wiley/IEEE Press books on mobile radio communications totalling in excess of 10 000 pages, published 1400+research entries at IEEE Xplore, acted both as TPC and General Chair of IEEE conferences, presented keynote lectures and has been awarded a number of distinctions. Currently he is directing a 100-strong academic research team, working on a range of research projects in the field of wireless multimedia communications sponsored by industry, the Engineering and Physical Sciences Research Council (EPSRC) UK, the European Research Council's Advanced Fellow Grant and the Royal Society's Wolfson Research Merit Award. He is an enthusiastic supporter of industrial and academic liaison and he offers a range of industrial courses. He is also a Governor of the IEEE VTS. During 2008–2012 he was the Editor-in-Chief of the IEEE Press and a Chaired Professor also at Tsinghua University, Beijing. His research is funded by the European Research Council's Senior Research Fellow Grant. For further information on research in progress and associated publications please refer to http://www-mobile.ecs.soton.ac.uk Lajos has 20 000+citations. AQ2

AUTHOR QUERIES

AUTHOR PLEASE ANSWER ALL QUERIES

AQ1 = Please provide field of membership year.
AQ2 = Please provide field of membership year.

END OF ALL QUERIES